

*Technical Report No. 32-349*

*Comparison of Calculated with Measured  
Boundary-Layer Thicknesses  
on the Curved Walls of the  
JPL 20-in. Supersonic Wind Tunnel  
Two-Dimensional Nozzle*

*Bain Dayman, Jr.*



JET PROPULSION LABORATORY  
CALIFORNIA INSTITUTE OF TECHNOLOGY  
PASADENA, CALIFORNIA

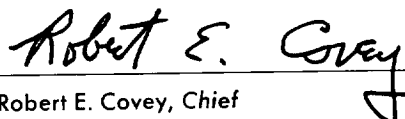
March 18, 1963



*Technical Report No. 32-349*

*Comparison of Calculated with Measured  
Boundary-Layer Thicknesses  
on the Curved Walls of the  
JPL 20-in. Supersonic Wind Tunnel  
Two-Dimensional Nozzle*

*Bain Dayman, Jr.*



Robert E. Covey, Chief  
Aerodynamic Facilities Section

JET PROPULSION LABORATORY  
CALIFORNIA INSTITUTE OF TECHNOLOGY  
PASADENA, CALIFORNIA

March 18, 1963

Copyright © 1963  
Jet Propulsion Laboratory  
California Institute of Technology

Prepared Under Contract No. NAS 7-100  
National Aeronautics & Space Administration

## CONTENTS

I. Introduction . . . . .	1
II. Experimental Local Skin-Friction of the Turbulent Boundary Layer over an Adiabatic Flat Plate . . . . .	2
III. Calculation of the Boundary Layer in the JPL 20-in. SWT . . . . .	4
IV. Conclusions . . . . .	12
Appendixes . . . . .	13
A. $R_0$ vs. $R_x$ Relationships . . . . .	13
B. Short-Cut Method of Estimating Test-Section Boundary-Layer Momentum and Displacement Thicknesses . . . . .	18
References . . . . .	22
Nomenclature . . . . .	23

## TABLES

1. JPL 20-in. SWT test-section boundary-layer measurements on centerline of curved wall . . . . .	5
2. Calculated values of test-section boundary-layer thicknesses using Eq. (3) . . . . .	6
3. Calculated values of test-section boundary-layer thicknesses using Eq. (2) . . . . .	6
A-1. Adiabatic flat-plate, turbulent-boundary-layer properties using Eq. (3) . . . . .	15
A-2. Effects of $\theta_0$ and $R/in.$ on calculations of $R_0$ using Eq.(3) . . . . .	15
A-3. Adiabatic flat-plate, turbulent-boundary-layer properties using Eq. (2) . . . . .	17
A-4. Percent error of $R_0$ vs. $R_x$ of Eq. (A-2) in matching data of Table A-3 . . . . .	18
B-1. JPL 20-in. SWT test-section boundary-layer measurements on centerline of curved wall . . . . .	20
B-2. JPL 12-in. SWT test-section boundary-layer measurements on centerline of curved wall . . . . .	20
B-3. CWT test-section boundary-layer measurements on centerline of curved wall . . . . .	21
B-4. AEDC 40-in. SWT test-section boundary-layer measurements on centerline of curved wall . . . . .	21

## FIGURES

1. Measured local skin-friction coefficient of the turbulent boundary layer over an adiabatic flat plate; $C_{f_m}/C_{f_i}$ vs. $R_o$ . . . . .	2
2. Analytic local skin-friction coefficient of the Schultz-Grunow incompressible turbulent boundary layer over an adiabatic flat plate; $C_{f_i}$ vs. $R_o$ . . . . .	2
3. Measured local skin-friction coefficient of the turbulent boundary layer over an adiabatic flat plate; $C_f/C_{f_i}$ vs. Mach number . . . . .	3
4. Analytic local skin-friction coefficient of the turbulent boundary layer over an adiabatic flat plate; $C_f/C_{f_i}$ vs. $R_o$ . . . . .	3
5. Mach number distribution along the curved walls of the JPL 20-in SWT . . . . .	4
6. Normalized values of the measured boundary-layer parameter, $H$ , in the JPL 20-in. SWT . . . . .	5
7. Analytic value of the turbulent boundary-layer parameter, $H_o$ . . . . .	6
8. Comparison of the local skin-friction coefficients, in Refs. 10 and 12, of the turbulent boundary layer over an adiabatic flat plate . . . . .	7
9. $C_f/C_{f_i}$ vs. $R_o$ regimes for the calculations of the curved-wall boundary layer for the JPL 20-in. SWT nozzle (high supply-pressure cases) . . . . .	7
10. $C_f/C_{f_i}$ vs. $R_o$ regimes for the calculations of the curved-wall boundary layer for the JPL 20-in. SWT nozzle (low supply-pressure cases) . . . . .	8
11. Calculated values of the boundary-layer momentum thickness along the curved nozzle wall of the JPL 20-in. SWT (high supply-pressure cases) . . . . .	8
12. Calculated values of the boundary-layer displacement thickness along the curved nozzle wall of the JPL 20-in. SWT (high supply-pressure cases) . . . . .	9
13. Calculated values of the boundary-layer momentum thickness along the $M = 3$ curved nozzle wall of the JPL 20-in. SWT (high vs. low supply-pressure cases) . . . . .	9
14. Calculated values of the boundary-layer displacement thickness along the $M = 3$ curved nozzle wall of the JPL 20-in. SWT (high vs. low supply-pressure cases) . . . . .	10
15. Calculated throat boundary-layer momentum-thickness as a function of Mach number . . . . .	10
16. Effect of chosen value of nozzle throat boundary-layer momentum thickness upon calculated value of test-section boundary-layer momentum thickness (high supply-pressure cases) . . . . .	10

## FIGURES (Cont'd)

17. Proportional effect of chosen value of nozzle-throat boundary-layer momentum thickness upon calculated value of test-section boundary-layer momentum thickness as a function of Mach number (high supply-pressure cases) . . . . .	11
A-1. $C_t/C_{t_i}$ vs. $M$ . . . . .	13
A-2. $R_\theta$ vs. $R_x$ as a function of Mach number [see Eq. (A-2)] . . . . .	14
B-1. $\theta_{tp}/\theta_m$ vs. $M$ for several supersonic wind tunnels . . . . .	19
B-2. Normalized values of the measured boundary-layer parameter, $H$ , from several supersonic wind tunnels . . . . .	19





## ABSTRACT

Experimentally determined values of the local skin-friction coefficients of adiabatic flat-plate, turbulent, compressible boundary layers were approximated by an analytical expression which, in turn, was used in conjunction with the boundary-layer integral-momentum equation to calculate test-section boundary-layer thicknesses in the Jet Propulsion Laboratory 20-in. Supersonic Wind Tunnel. These calculations were compared with measured boundary-layer thicknesses for the Mach number range of 1.4 to 5. These comparisons were fair, but varied as the Reynolds number was varied. The use of a simpler, analytical boundary-layer skin-friction equation gave better comparisons and was not as dependent upon Reynolds number as the somewhat less simple analytical expression. A short-cut method (in contrast to the step-by-step integration from the throat to the test section) for estimating the test-section boundary-layer momentum and displacement thicknesses is shown, and several examples are given.

## I. INTRODUCTION

Many experimenters have measured the local skin-friction of adiabatic flat-plate, turbulent boundary layers in the ranges of  $1.5 < M < 5.8$  and  $10^3 < R_\theta < 1.5 \times 10^4$  (see Refs. 1-7). Since very careful measurements of the Jet Propulsion Laboratory (JPL) 20-in. Supersonic Wind Tunnel (SWT) test-section boundary layer have been made for  $1.4 < M < 5$  (mainly on the centerline of the two-dimensional nozzle curved walls; see Ref. 8) it seemed appropriate to determine the degree of compatibility of these two types of measurements when related by means of the boundary-layer integral momentum equation.

The procedure followed was: (a) to establish a simple analytical expression for the local skin friction from a turbulent boundary layer over an experimental flat plate, (b) to use experimental boundary-layer displacement-thickness to boundary-layer momentum-thickness ratios, and then (c) to apply the boundary-layer integral momentum equation using the designed Mach-number distribution along the curved walls of the JPL 20-in. SWT. This was done for test-section Mach numbers of 1.4, 1.64, 2, 3, 4, and 5 at maximum tunnel supply pressures, and for  $M = 2, 3$ , and 4 at considerably decreased supply pressures.

## II. EXPERIMENTAL LOCAL SKIN-FRICTION OF THE TURBULENT BOUNDARY LAYER OVER AN ADIABATIC FLAT PLATE

Figure 1 presents the experimental local skin-friction of the turbulent boundary layer over an adiabatic flat plate (Refs. 1-7) as a function of the momentum-thickness Reynolds number. The skin-friction data were normalized by being ratioed to the corresponding Schultz-Grunow data on the local skin friction of an incompressible, turbulent boundary layer over an adiabatic flat plate (Ref. 9) as shown in Fig. 2.

$$C_{fi} = \frac{0.0334}{(\log_{10} R_\theta)^{1.838}} \quad (1)$$

The experimental data shown in Fig. 1 were faired with straight lines of equal slopes, which in turn were cross-plotted in Fig. 3, giving good agreement with the analytical, Mach-number-dependent, local skin-friction equation (Ref. 10).

$$\frac{C_f}{C_{fi}} = (1 + 0.144 M^2)^{-0.578} \quad (2)$$

The data in Figs. 2 and 3 were then approximated by the Mach- and Reynolds-number-dependent expression [Eq. (3)], the result being shown in Fig. 4.

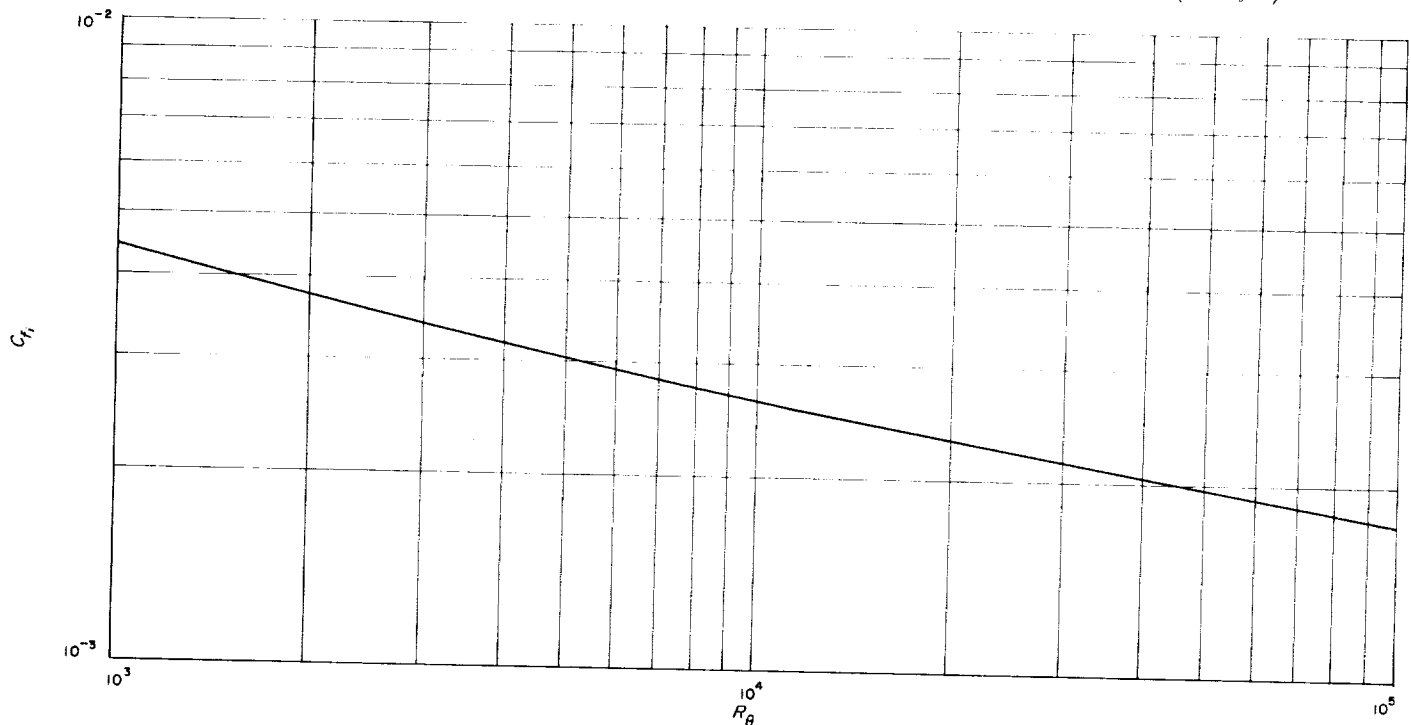


Fig. 2. Analytic local skin-friction coefficient of the Schultz-Grunow incompressible turbulent boundary layer over an adiabatic flat plate;  $C_{fi}$  vs.  $R_\theta$

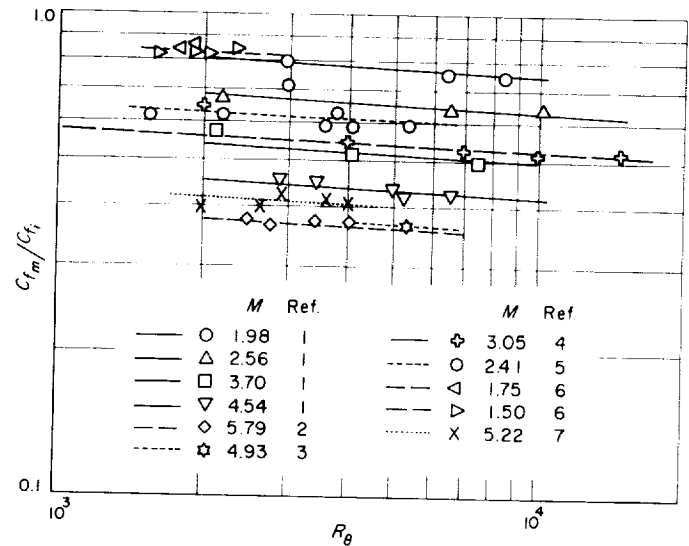


Fig. 1. Measured local skin-friction coefficient of the turbulent boundary layer over an adiabatic flat plate;  $C_{fm}/C_{fi}$  vs.  $R_\theta$

$$\frac{C_f}{C_{fi}} = (1 + 0.144 M^2)^{-0.578} \times \left( \frac{2 \times 10^3}{R_\theta} \right)^{0.05} \quad (3)$$

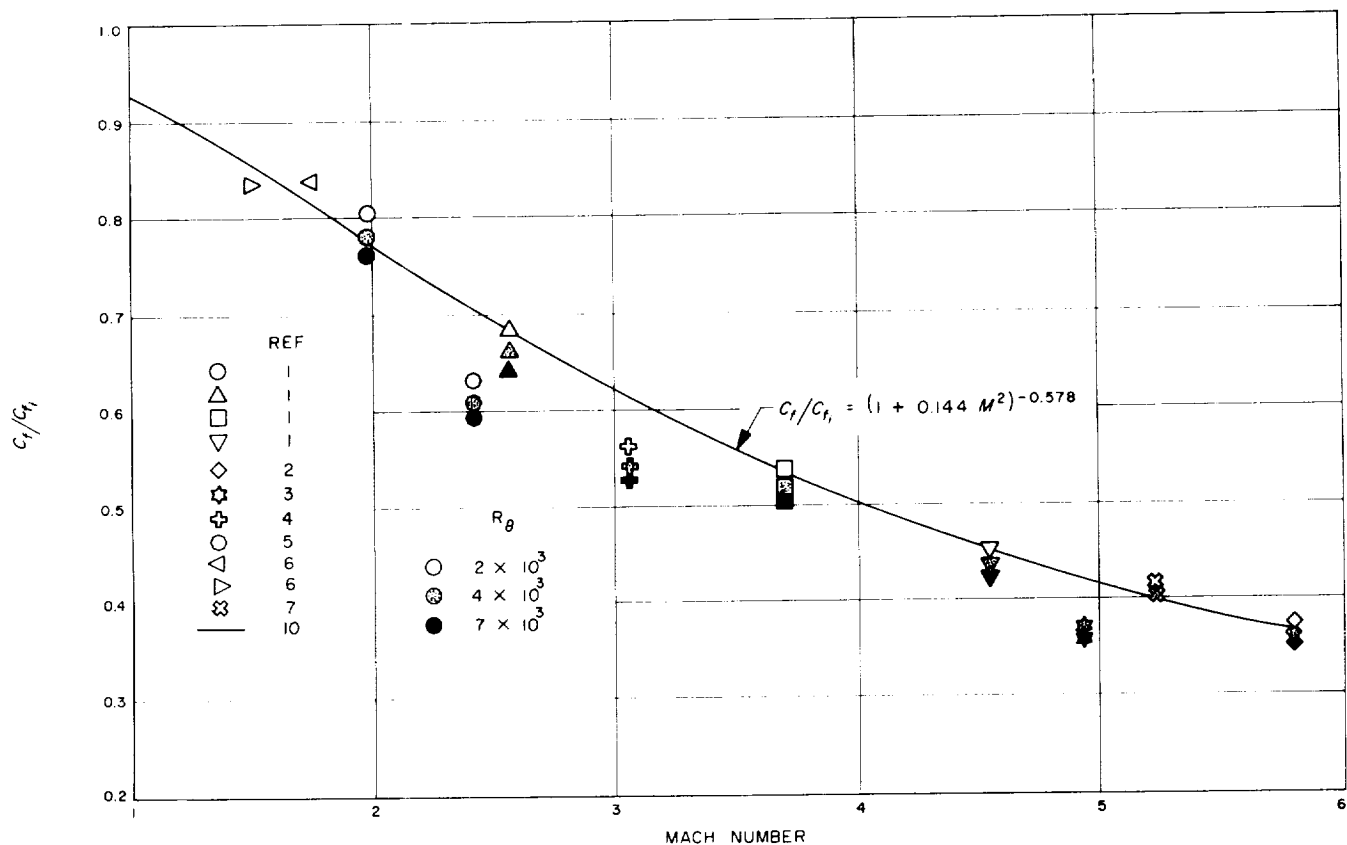


Fig. 3. Measured local skin-friction coefficient of the turbulent boundary layer over an adiabatic flat plate;  $C_t/C_{t_i}$  vs. Mach number

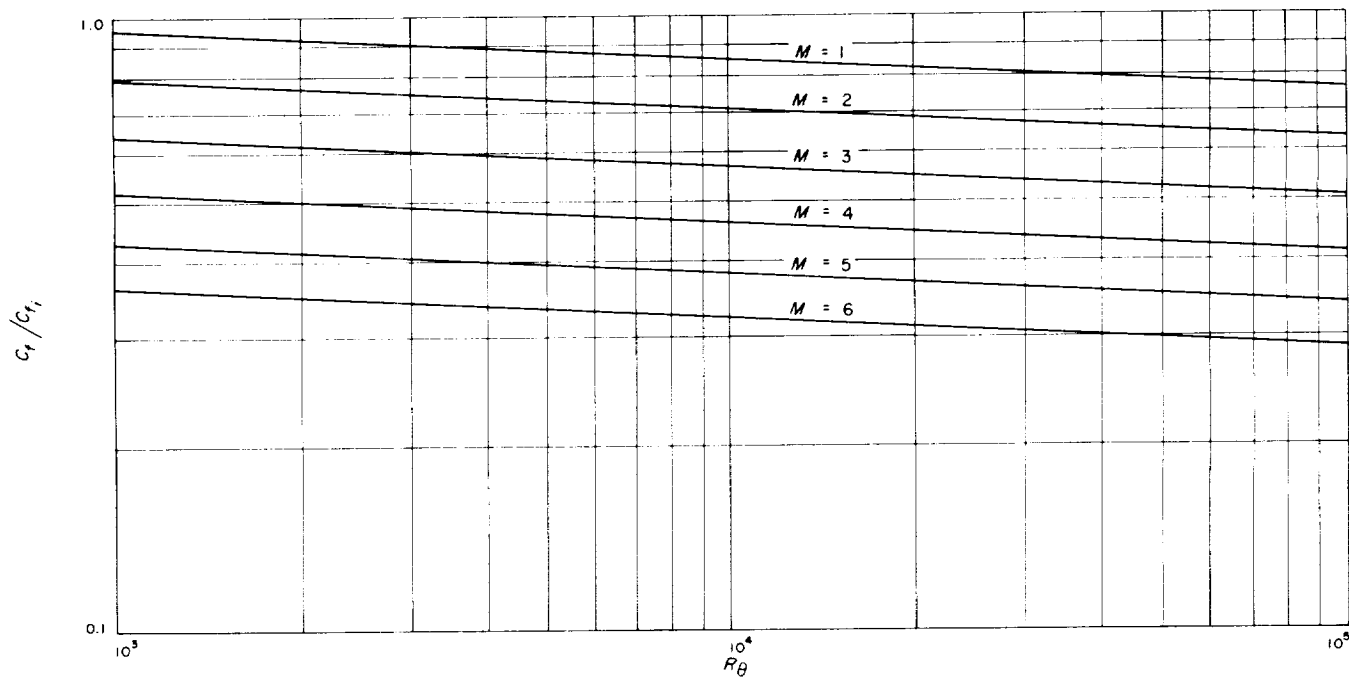


Fig. 4. Analytic local skin-friction coefficient of the turbulent boundary layer over an adiabatic flat plate;  $C_t/C_{t_i}$  vs.  $R_\theta$

### III. CALCULATION OF THE BOUNDARY LAYER IN THE JPL 20-IN. SWT

The distribution of the Mach number along a curved wall of the JPL 20-in. SWT two-dimensional nozzle is shown in Fig. 5 along with the location of the downstream end of the curved wall. The boundary-layer momentum thickness at the nozzle throat was obtained by the method used in Ref. 11.

$$\theta_0 \text{ (ft)} = 5.06 \times 10^{-3} \frac{(\nu^*)^{1/5} \times (t^* L^*)^{2/5}}{(T_t)^{1/10}} \quad (4)$$

The values of  $\theta_0$  used are listed in Table 1 along with data from Ref. 8.

The one relation left to determine before being able to use the boundary-layer integral-momentum equation [Eq. (5)] is the variation of the boundary-layer displacement to momentum thickness ( $H$ ).

$$\frac{d\theta}{dx} = \frac{C_f}{2} - \frac{dM}{dX} \times \left[ \frac{2-M^2+H}{M(1+0.2M^2)} \right] \theta \quad (5)^a$$

The variation of test-section  $H$  with Mach number and, to a limited degree, with Reynolds number was obtained from the data of Table B-1 in Appendix B (see Ref. 8; the value of  $H$  at the throat is included from Ref. 11). This variation, shown in Fig. 6, was normalized by ratioing it to the  $H_0$  value of Ref. 10, which is plotted in Fig. 7.

$$H_0 = 1.3 + 0.46 M^2 \quad (6)^a$$

The ratio  $H/H_0$  increases with decreasing Reynolds number, and remains relatively constant for  $M > 2.5$ . The total excursion of  $H/H_0$  throughout the Mach number range, for the maximum supply pressure case, is from 0.96 to 1.02, a total variation of only 6%. In the integration of Eq. (5), the value  $H/H_0$  was made a constant, dependent upon each nozzle Mach number and the supply pressure condition (high or low). These values of  $H/H_0$  were chosen to be somewhat of an average from the throat to the test section, and are listed in Table 1. The integration of Eq. (5) is not particularly sensitive to the chosen ratio of  $H/H_0$ , a 3% variation giving only a 1% change in the test section boundary-layer momentum thickness (in the opposite direction) for the  $M = 3$  nozzle. Of course, the boundary-layer displacement thickness will then be changed by 2% (in the same direction as the change in the  $H/H_0$  ratio).

The results of these wind-tunnel nozzle, boundary-layer thickness calculations are shown in Table 2, where they are compared with the measured values. As can be seen, the calculated values of the boundary-layer thicknesses

<sup>a</sup>In air for  $\gamma = 1.4$ .

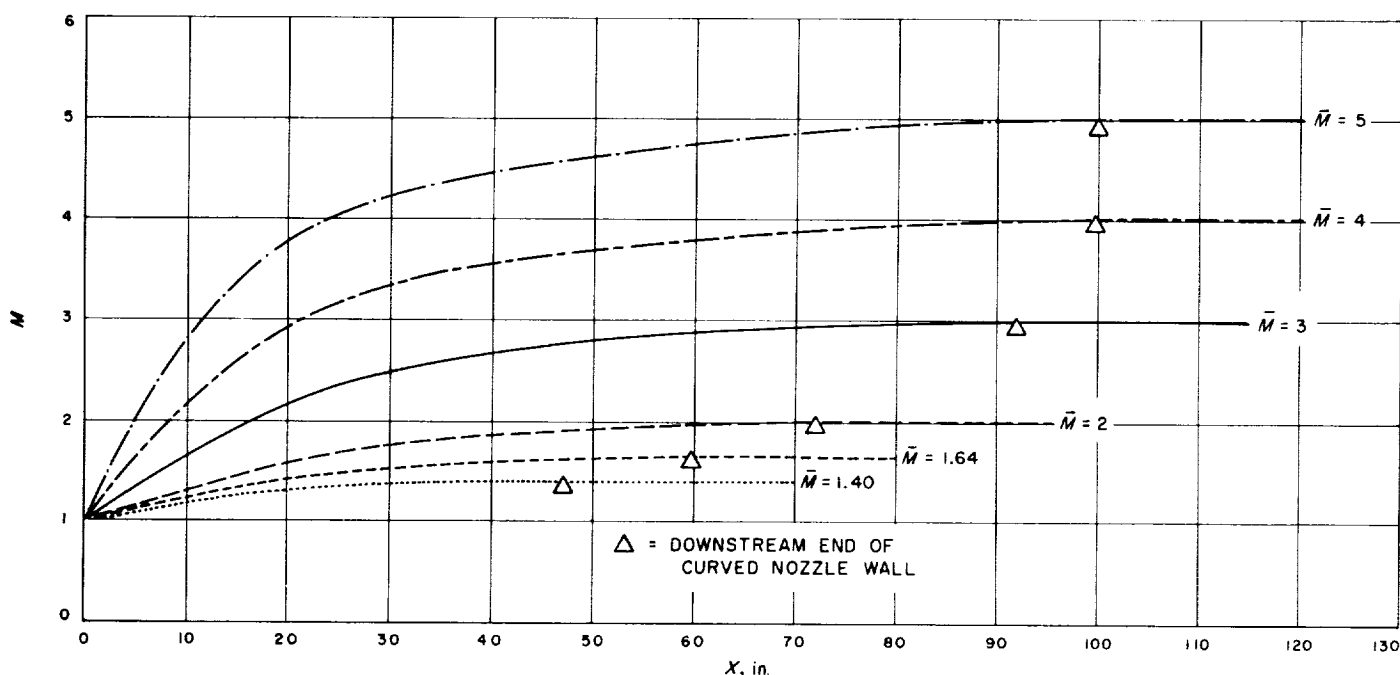


Fig. 5. Mach number distribution along the curved walls of the JPL 20-in. SWT

Table 1. JPL 20-in. SWT test-section boundary-layer measurements  
on centerline of curved wall

$M$	$P_t$ cm Hg	$T_t$ °R	$R/\text{in.}$ $\times 10^{-5}$	$x$ in.	$r^*$ in.	$L^*$ in.	$\delta_m^*$ in.	$\theta_m$ in.	$H_m$	$\theta_0^{a,b}$ in.	$H^{*,c}/H_0$
1.4	110	570	5.10	66.1	17.8	226	0.171	0.0769	2.23	0.0222	1.00
1.64	115	573	4.99	78.9	15.3	174	0.201	0.0797	2.52	0.0188	1.01
2	34	540	1.39	92.4	11.5	126	0.302	0.0958	3.15	0.0185	1.01
2	135	580	5.01	92.4	11.5	126	0.249	0.0804	3.10	0.0143	0.99
3	56	538	1.38	112.0	4.43	69	0.548	0.1030	5.32	0.0090	0.99
3	150	579	3.32	112.0	4.43	69	0.476	0.0903	5.27	0.0075	0.97
4	90	558	1.23	118.9	1.69	52	0.883	0.1050	8.42	0.0050	0.99
4	255	580	3.29	118.9	1.69	52	0.765	0.0924	8.28	0.0041	0.97
5	330	605	2.45	118.4	0.715	52	1.136	0.0926	12.27	0.0028	0.97

<sup>a</sup>Parameters used in Eq. (5).

<sup>b</sup>From Eq. (4).

<sup>c</sup>Estimated effective average value throughout nozzle; from Fig. 6.

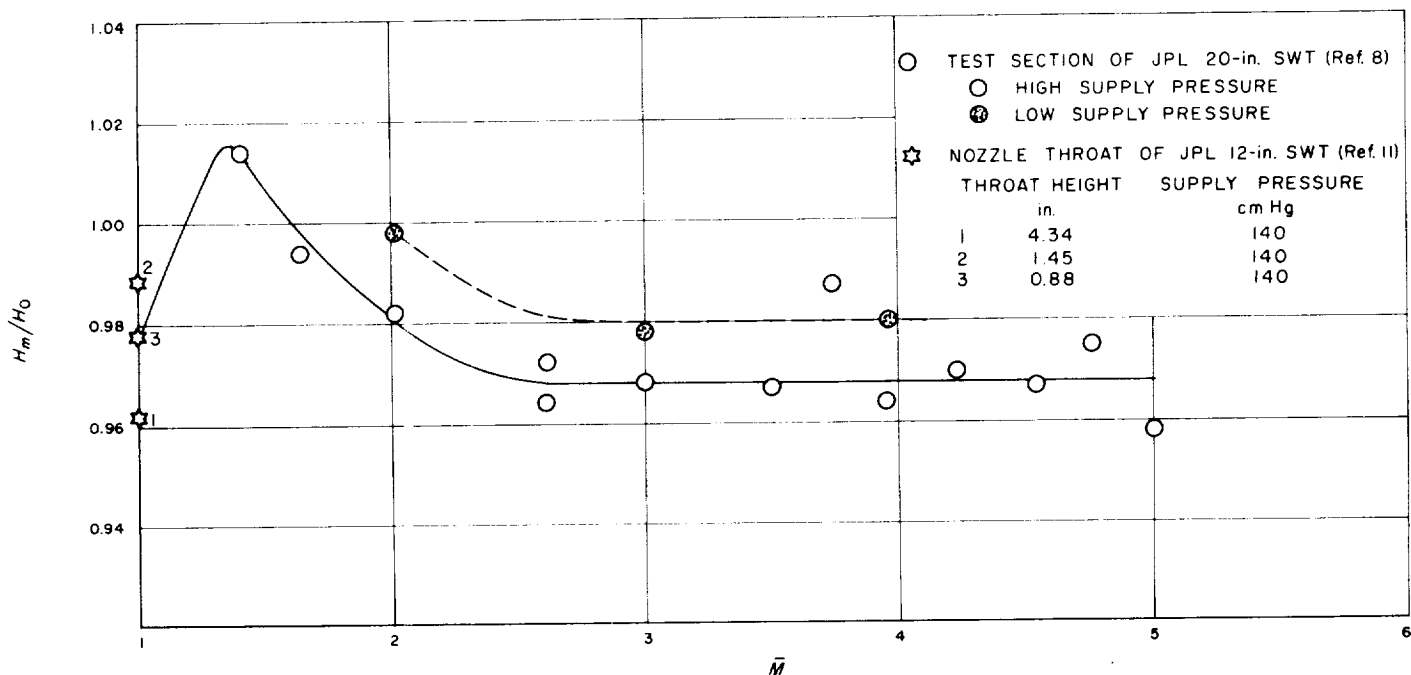


Fig. 6. Normalized values of the measured boundary-layer parameter,  $H$ , in the JPL 20-in. SWT

in the test section are too low, ranging from 15% low at  $M = 1.4$  to 7% low at  $M = 5$  for the high supply-pressure cases. It seems reasonable to expect that the comparisons (of the calculated values of boundary-layer thicknesses with the measured values) should be essentially the same, at each nozzle contour, for all values of supply pressure as long as the boundary layer is turbulent from the throat on. That is, any shortcomings in the application of the boundary-layer, integral momentum equation should apply equally as well to the high supply-pressure case as to the low supply-pressure case. As this is not the situa-

tion, and since the calculations for the low supply-pressure cases were in considerably better agreement with the measured values than they were in the high-pressure cases, the use of the experimental data of Fig. 1, which decreases with increasing Reynolds number, does not appear to be appropriate for use in wind-tunnel boundary-layer calculations. Perhaps the problem with these data is even more basic: they should not have been assumed to be Reynolds-number dependent (although, in general, they do appear to exhibit such a trend), but rather a best-level, straight-line fairing should have been made.

It becomes clear that more consistent calculations would result if the ratio of  $C_f/C_{f_i}$  did not drop off with increasing Reynolds number. For this reason, the nozzle boundary-layer calculations were repeated using Eq. (2) [rather than Eq. (3)] with Eqs. (5) and (6), the results being listed in Table 3. For the high supply-pressure case, the

**Table 2. Calculated values of test-section boundary-layer thicknesses using Eq. (3)**

$M$	$P_t$	$\theta$ in.	$\delta^*$ in.	$\frac{\theta}{\theta_m}$	$\frac{\delta^*}{\delta_m^*}$
1.4	High	0.0653	0.144	0.850	0.843
1.64	High	0.0680	0.174	0.853	0.866
2	Low	0.0917	0.290	0.958	0.962
2	High	0.0715	0.222	0.888	0.892
3	Low	0.0995	0.536	0.966	0.978
3	High	0.0841	0.444	0.932	0.934
4	Low	0.1018	0.873	0.970	0.988
4	High	0.0844	0.709	0.914	0.928
5	High	0.0857	1.065	0.926	0.938

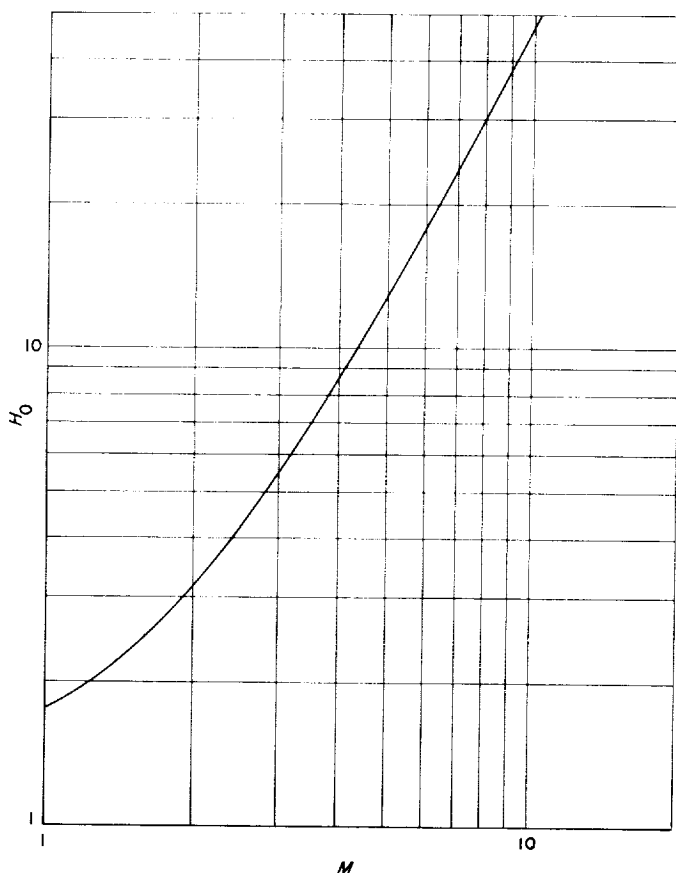


**Fig. 7. Analytic value of the turbulent boundary-layer parameter,  $H_0$**

**Table 3. Calculated values of test-section boundary-layer thicknesses using Eq. (2)**

$M$	$P_t$	$\theta$ in.	$\delta^*$ in.	$\frac{\theta}{\theta_m}$	$\frac{\delta^*}{\delta_m^*}$
1.4	High	0.0711	0.157	0.924	0.918
1.64	High	0.0744	0.191	0.934	0.950
2	Low	0.0966	0.306	1.008	1.013
2	High	0.0785	0.244	0.976	0.980
3	Low	0.1051	0.566	1.020	1.033
3	High	0.0914	0.483	1.012	1.015
4	Low	0.1072	0.919	1.021	1.041
4	High	0.0918	0.771	0.993	1.008
5	High	0.0918	1.140	0.992	1.004

calculated values of the boundary-layer thicknesses range from 8% low at  $M = 1.4$  to 2% high at  $M = 3$  in comparison with the measured values. Although the range of disagreement from the measured values is not improved over that when Eq. (3) was used, at least it now brackets unity—a very desirable result. In addition, the effect of Reynolds number upon the comparison has been considerably reduced. Certainly it would be possible to come up with a  $C_f/C_{f_i}$  vs.  $R_x$  relationship that would make the calculated values of boundary-layer thickness agree almost exactly with the measured values, but for all practical purposes, the comparisons by use of Eq. (2) are adequate. Only at the two lower nozzle Mach numbers ( $M = 1.4, 1.64$ ) are the discrepancies large (5 to 8%), and it is here that they are least important because the boundary-layer displacement thickness is such a small part of the nozzle height in comparison to the higher Mach-number nozzles.

The  $C_f/C_{f_i}$  values of Eq. (2) are compared with those of Ref. 12 in Fig. 8. The comparison is quite favorable for  $M < 3$ , but at  $M = 6$  there is a rather large discrepancy of about 25%. It is not the intent of this Report to discuss the validity of one Reference over another, but rather to show that care must be used in choosing the local skin-friction law for the turbulent boundary layers over an adiabatic flat plate when calculating wind-tunnel nozzle boundary layers.

Figures 9 and 10 indicate the portions of the  $C_f/C_{f_i}$  vs.  $R_x$  regions that are used in the calculation of the boundary-layer growth along the nozzle. Upon comparison of these two figures with Fig. 1 it becomes apparent that for the high supply-pressure case, the major portion of the boundary-layer growth takes place beyond the  $R_x$  region of experimental values of  $C_f/C_{f_i}$  while the lower pressure case is in the region of experimental, local skin-friction measurements.

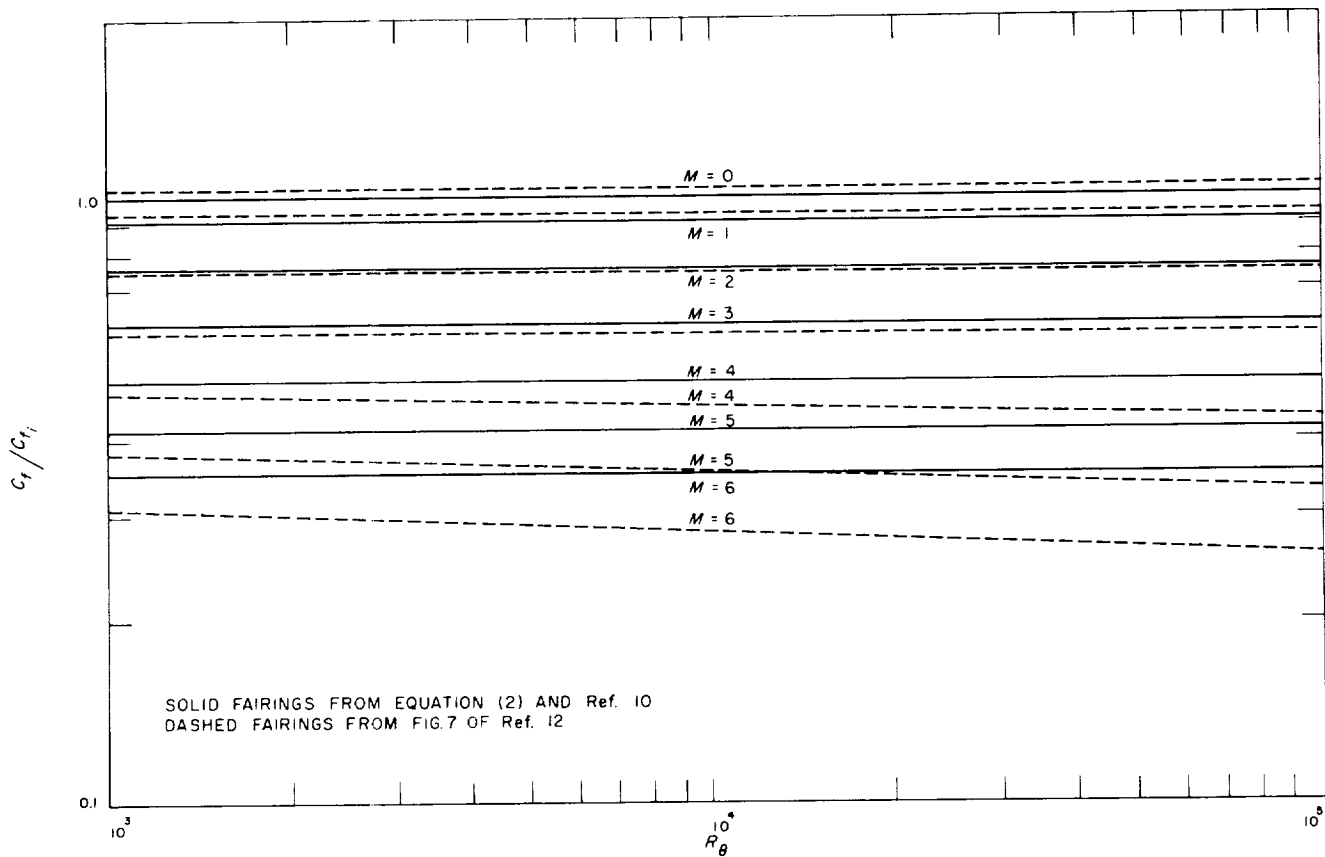


Fig. 8. Comparison of the local skin-friction coefficients, in Refs. 10 and 12, of the turbulent boundary layer over an adiabatic flat plate

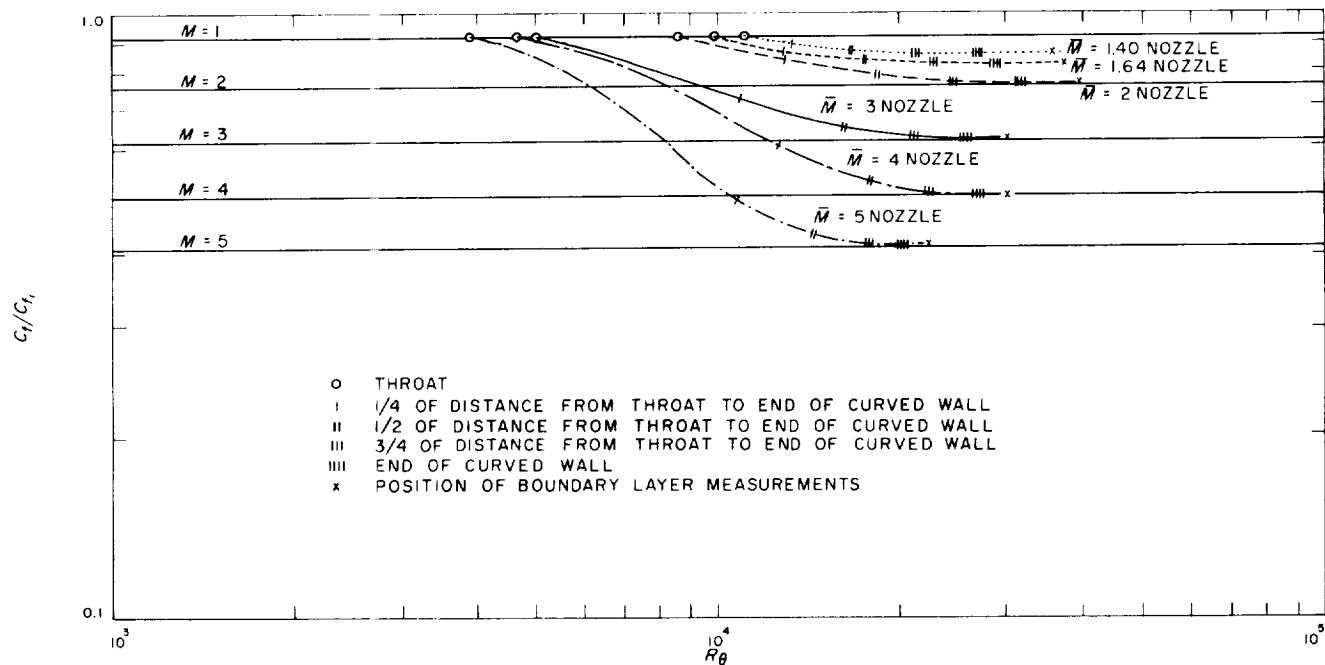


Fig. 9.  $C_t/C_{t_i}$  vs.  $R_\theta$  regimes for the calculations of the curved-wall boundary layer for the JPL 20-in. SWT nozzle (high supply-pressure cases)

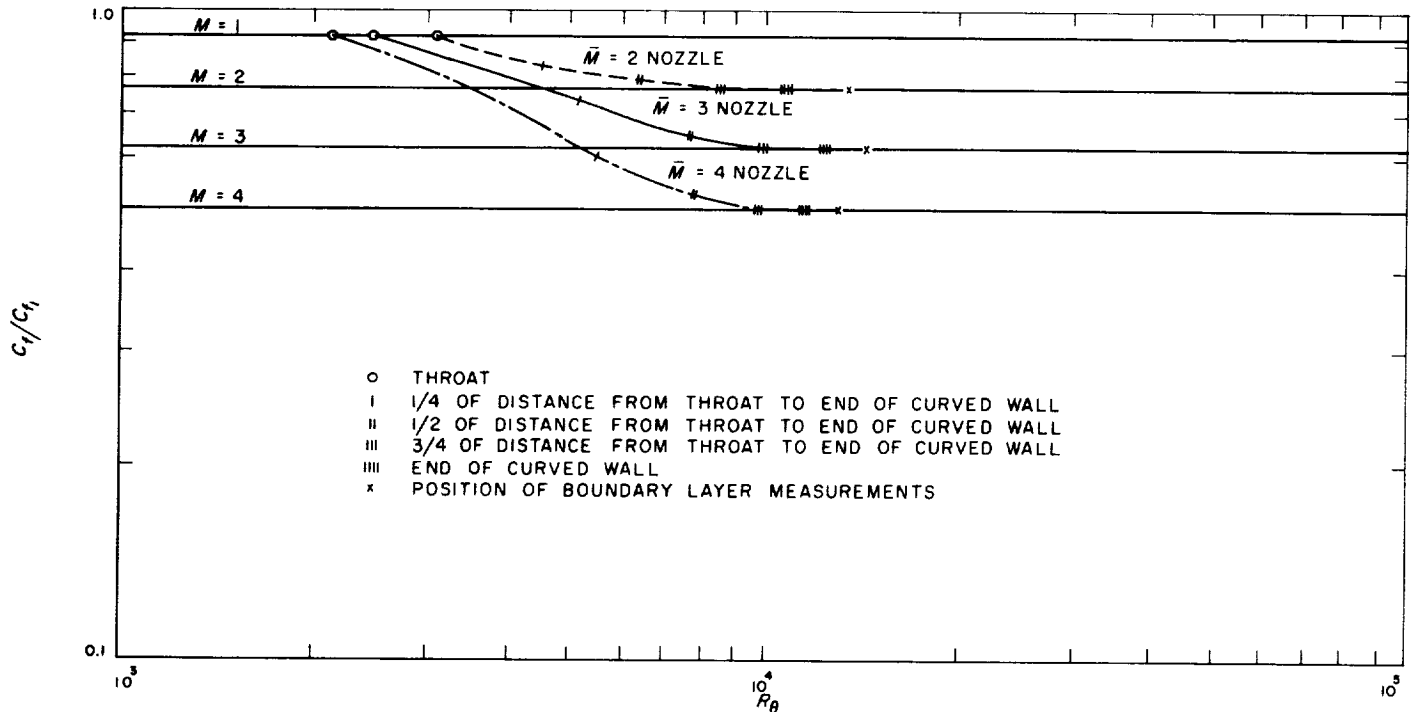


Fig. 10.  $C_t/C_{t1}$  vs.  $R_\theta$  regimes for the calculations of the curved-wall boundary layer for the JPL 20-in. SWT nozzle (low supply-pressure cases)

The results of the boundary-layer calculations along the nozzle using Eqs. (2), (5), and (6) are shown in Figs. 11 and 12 and are compared with the measured values in the test section at the high supply-pressure condition. Com-

parison of these two figures (and Figs. 13 and 14) with Fig. 5 shows that the major portion of the boundary-layer growth for each nozzle takes place at Mach numbers very much closer to the test-section Mach number than to the

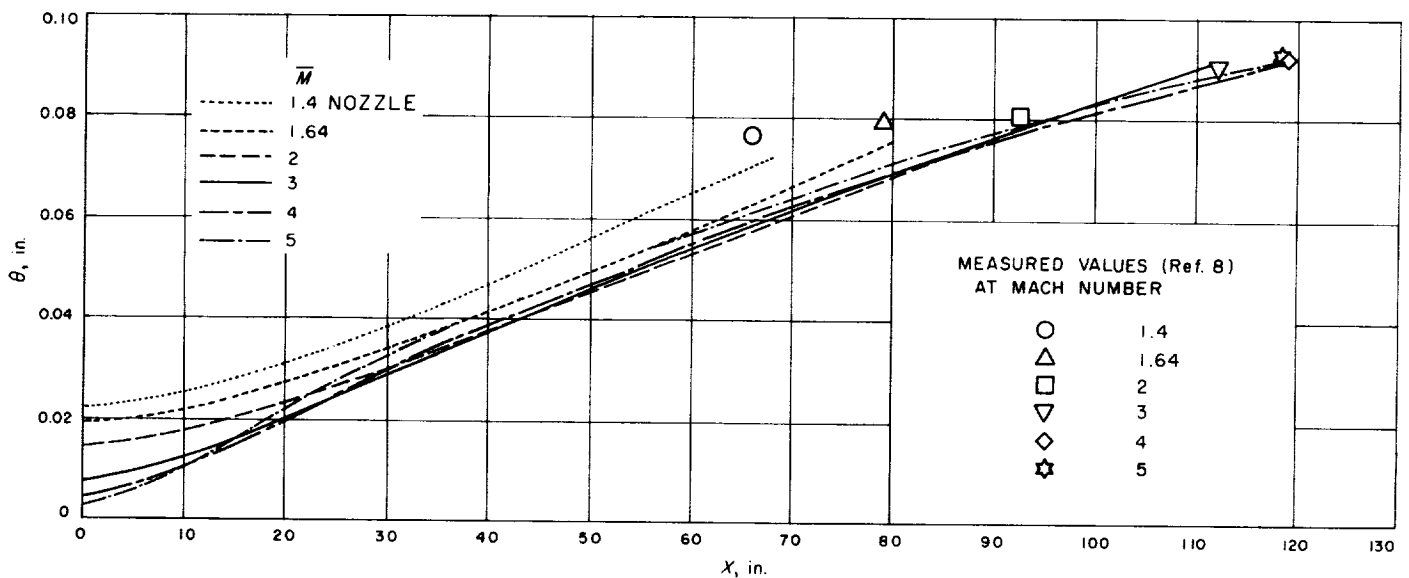


Fig. 11. Calculated values of the boundary-layer momentum thickness along the curved nozzle wall of the JPL 20-in. SWT (high supply-pressure cases)



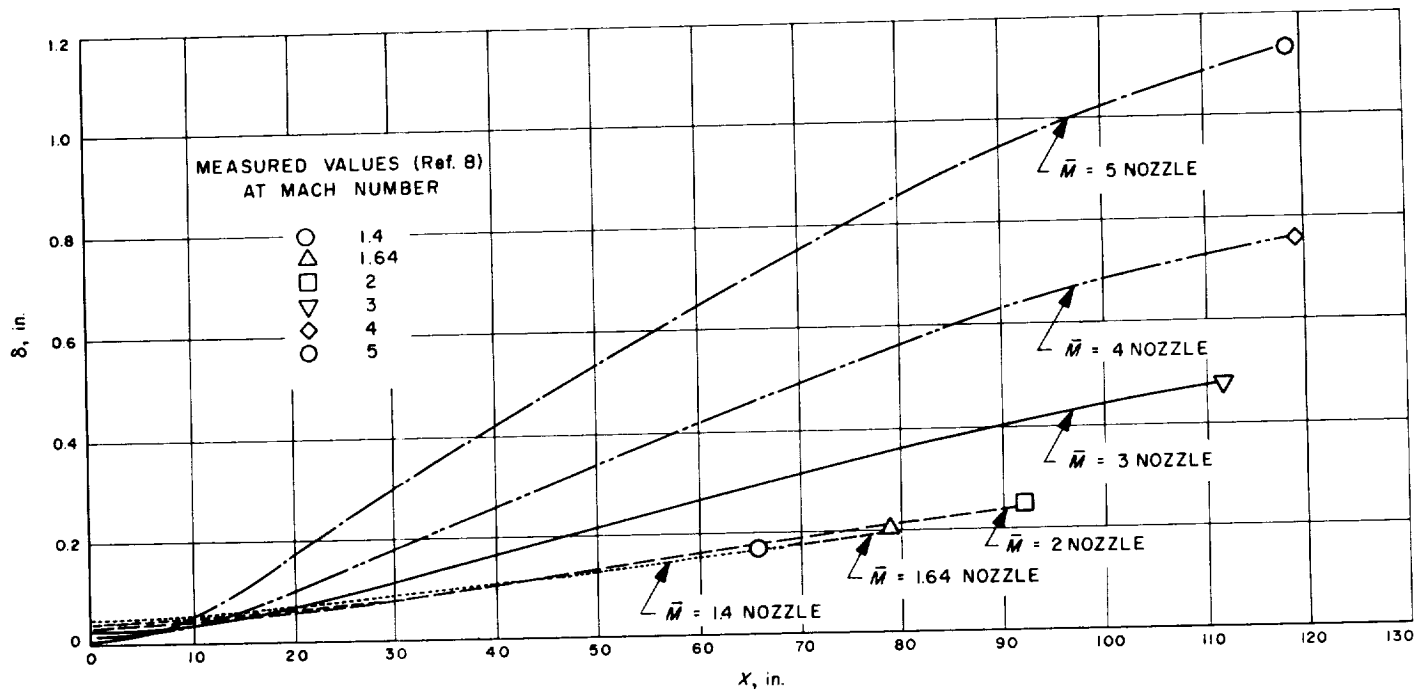


Fig. 12. Calculated values of the boundary-layer displacement thickness along the curved nozzle wall of the JPL 20-in. SWT (high supply-pressure cases)

throat Mach number of  $M = 1$ . The effect of the supply pressure (high vs. low) upon the boundary-layer growth of the  $M = 3$  nozzle is shown in Figs. 13 and 14.

Figure 15 shows the value of  $\theta_0$  [as calculated with Eq. (4)] used for both the high and low supply-pressure cases. The effect on the test-section boundary-layer mo-

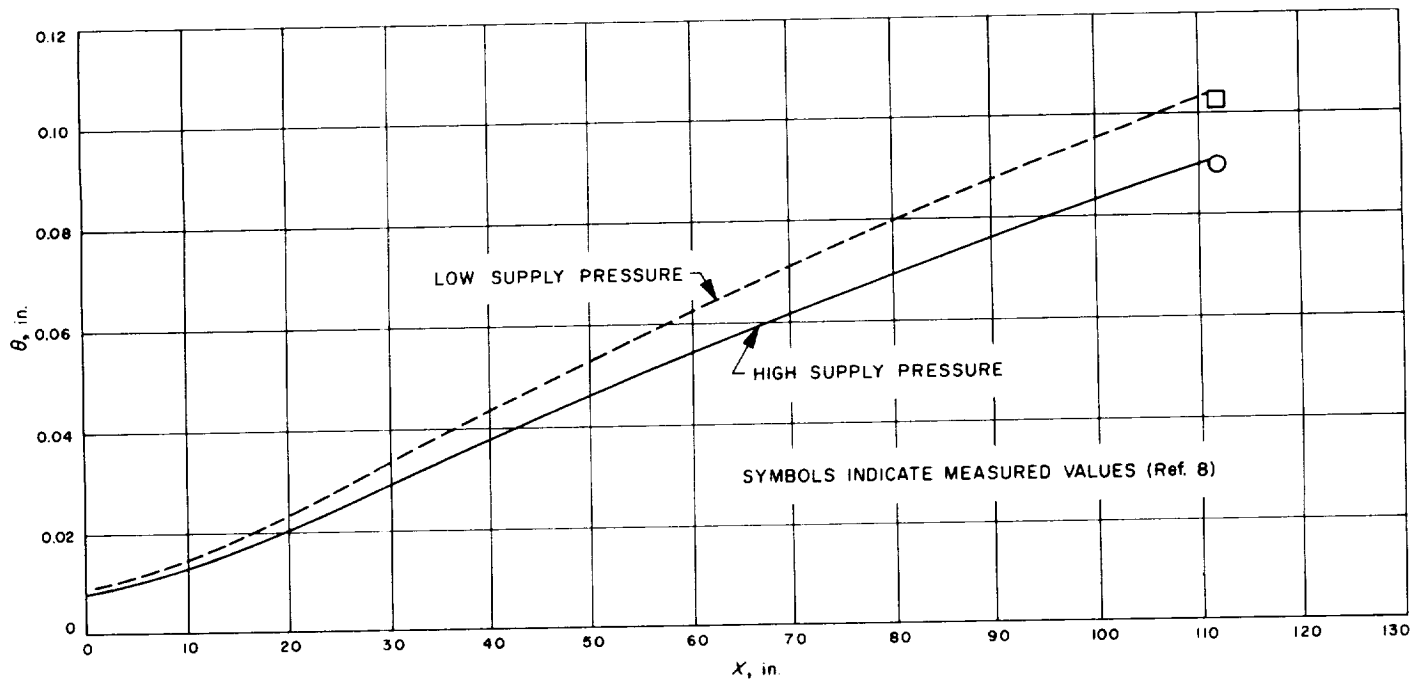


Fig. 13. Calculated values of the boundary-layer momentum thickness along the  $M = 3$  curved nozzle wall of the JPL 20-in. SWT (high vs. low supply-pressure cases)

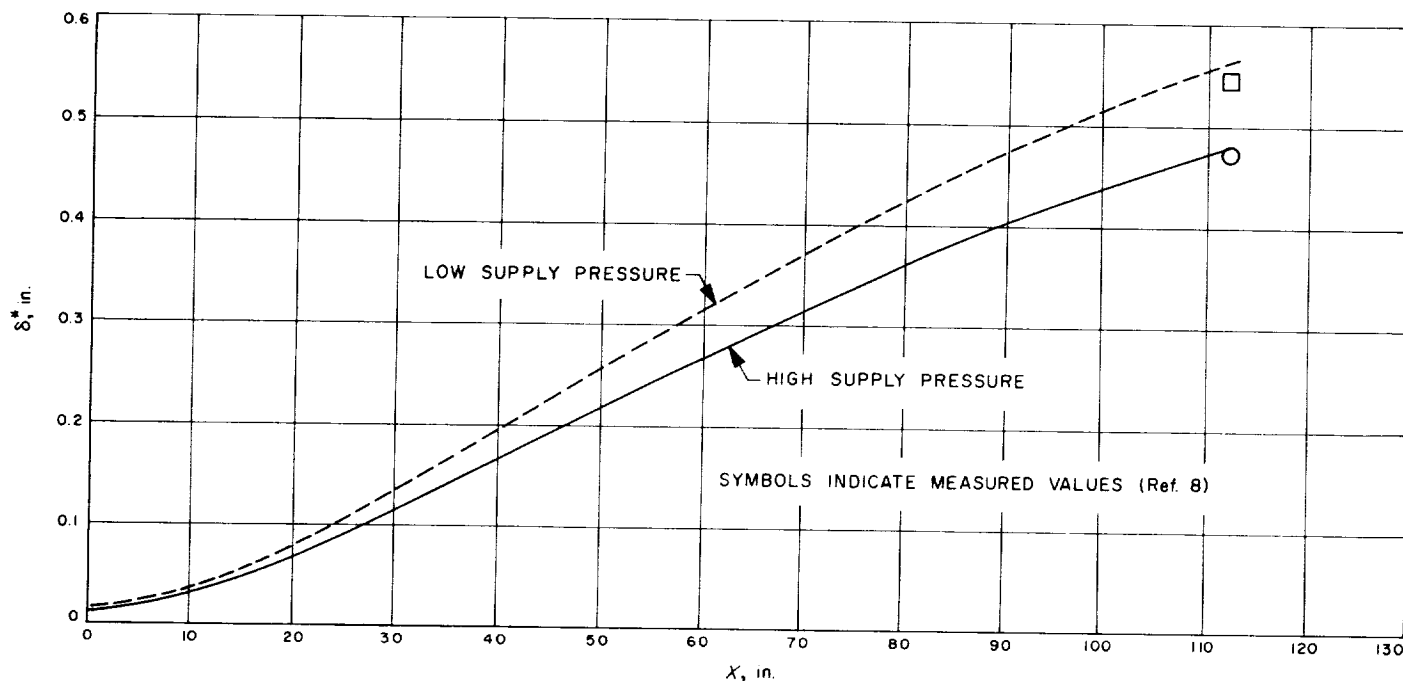


Fig. 14. Calculated values of the boundary-layer displacement thickness along the  $M = 3$  curved nozzle wall of the JPL 20-in. SWT (high vs. low supply-pressure cases)

mentum thickness (at the location of the measured values) of the chosen value for the throat momentum thickness

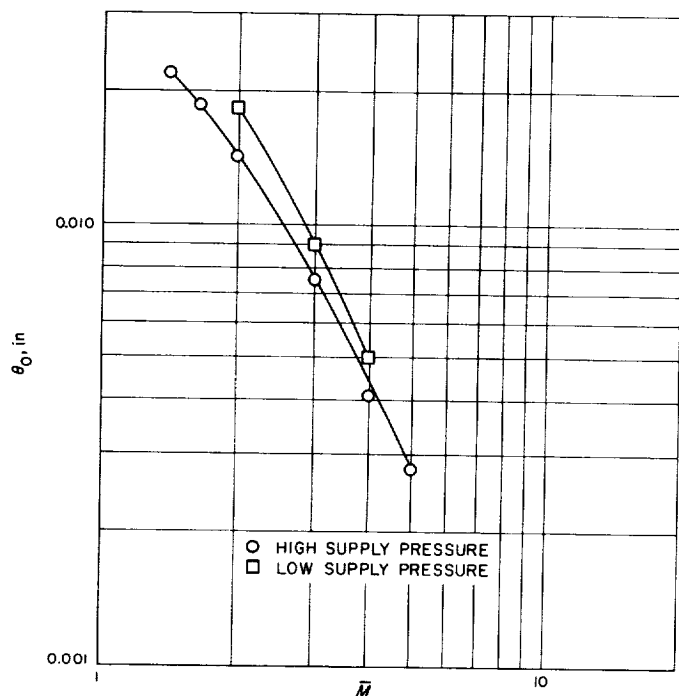


Fig. 15. Calculated throat boundary-layer momentum-thickness as a function of Mach number

is shown in Fig. 16 for the  $M = 1.4$  and  $M = 3$  nozzles (high supply-pressure case). At  $M = 1.4$  a 50% decrease or increase in  $\theta_0$  results in about a 5% decrease or increase in the test section  $\theta$ , while at  $M = 3$  a 100% increase in  $\theta_0$  results in only a  $1\frac{1}{2}\%$  increase in the test section  $\theta$ . Figure 17 presents the proportion change in test section  $\theta$  relative to a change of one  $\theta_0$  in throat mo-

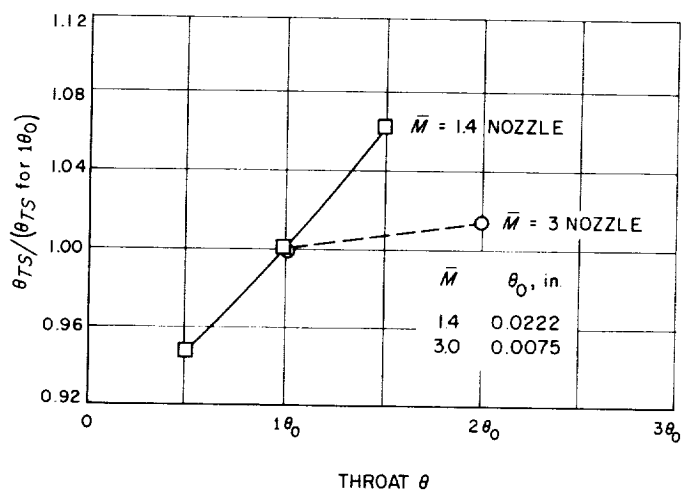


Fig. 16. Effect of chosen value of nozzle throat boundary-layer momentum thickness upon calculated value of test-section boundary-layer momentum thickness (high supply-pressure cases)

momentum thickness at  $\theta_0$ . Although theoretical data were obtained at only two nozzle Mach numbers, some liberty was taken in fairing these two points in order to demon-

strate the decreasing effect of the chosen  $\theta_0$  on the test section  $\theta$  which accompanies an increasing nozzle Mach number.

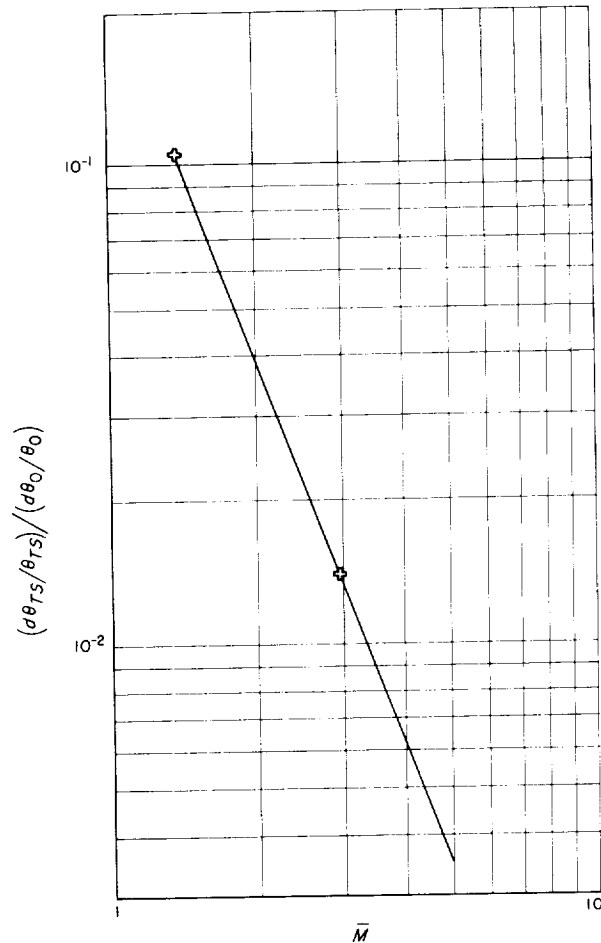


Fig. 17. Proportional effect of chosen value of nozzle-throat boundary-layer momentum thickness upon calculated value of test-section boundary-layer momentum thickness as a function of Mach number (high supply-pressure cases)

## IV. CONCLUSIONS

An analytical formulation was made of experimental, local-skin-friction data from the turbulent boundary layer over an adiabatic flat plate and was then applied to the boundary-layer growth along the curved walls of the JPL 20-in. Supersonic Wind Tunnel using the boundary-layer integral-momentum equation. The resulting test-section boundary-layer thicknesses were not consistent with measured thicknesses, being generally too small. However, the major problem was the variation with Reynolds number of the discrepancy between the calculated and measured values of the boundary-layer thickness as the Reynolds number was changed by a factor of three. This was true for several nozzle shapes.

In order to decrease this variation in discrepancy with Reynolds number, the simpler skin-friction formulation of Ref. 10 was used in the calculation of the boundary-layer growth along the nozzle. In addition, the agreement with measured values was considerably improved. For  $2 < M < 5$ , the calculated values of the boundary-layer momentum and displacement-thicknesses agree with the measured values to within 4%, even for variations of a factor of three in the Reynolds numbers. At the lowest Mach number of 1.4, the agreement is still within 8% — more than satisfactory for nozzle design.

The simple, adiabatic, flat-plate, turbulent-boundary-layer, local-skin-friction formula of Ref. 10 was integrated to give values of  $R_o$  vs.  $R_x$  for a flat plate. It was then

possible to derive an equation of  $R_o$  vs.  $R_x$  good to 2% for  $10^6 < R_x < 10^9$  and  $0 < M < 6$  (Appendix A). This equation then can be used to estimate the turbulent-boundary-layer momentum thickness on an adiabatic flat plate.

A comparison between the flat-plate boundary-layer (based upon the  $R_o$  vs.  $R_x$  equation, distance from nozzle throat to test section, and test-section unit Reynolds number) and the actual measured values in the JPL 20-in. SWT can be used to estimate test-section boundary layers on the curved walls in two-dimensional wind tunnels of various sizes (see Appendix B). Such a procedure gives boundary-layer momentum thicknesses that are generally within 5% of the measured values for the three tunnels investigated: the JPL 12-in. supersonic wind tunnel, with both  $9 \times 12$  and  $12 \times 12$ -in. test sections; the AEDC 40-in. SWT; and the CIT-CWT  $8\frac{1}{2} \times 11\frac{1}{4}$ -ft test section. The use of the JPL 20-in. SWT-measured ratio of boundary-layer displacement to momentum thickness gave corresponding values of displacement thicknesses of these three other tunnels which agree to within about 13% of the measured values. The tunnel scale appears to have a large effect on the  $\delta^*/\theta$  ratio even for the same value of  $R_x$ . The data of this investigation indicated a scale effect, and perhaps these data can be used for other tunnels to a higher degree of accuracy than is possible by using only the results from the JPL 20-in. SWT.

## APPENDIX A

 $R_o$  vs.  $R_x$  Relationships

In many adiabatic, flat-plate, turbulent-boundary-layer investigations, the relationship of the boundary-layer momentum-thickness Reynolds number ( $R_o$ ) as a function of the flat-plate-length Reynolds number ( $R_x$ ) is required. This relation can be obtained by integrating Eq. (A-1) using the experimental data skin friction formula of Eq. (3) for  $M = 0, 1, 2, 3, 4, 5$ , and 6.

$$\theta = \frac{1}{2} \int_0^x C_f dx \quad (\text{A-1})$$

The distance increments ( $\Delta x$ ) used for the integration of Eq. (A-1) were:

$x$ , in.	$\Delta x$ , in.
0 to 5	0.1
5 to 10	0.5
10 to 50	1
50 to 100	5
100 to 500	10
500 to 1000	50
1000 to 5000	100
5000 to 10000	500

With a unit Reynolds number of  $10^5$  per in., the value of the momentum thickness ( $\theta_o$ ) at the plate leading edge ( $x = 0$ ) was taken to be 0.001 in. The results of this integration are summarized in Table A-1.

The effect of varying the leading-edge momentum thickness ( $\theta_o$ ) was investigated by letting  $\theta_o = 0.003$  in., and is shown in Table A-2. At  $R_x = 10^6$ , the variation in  $R_o$  due to a change in  $\theta_o$  from 0.001 in. to 0.003 in. is about 5%, and at  $R_x = 10^7$  it is down to a negligible 1/2%. Therefore, the choice of  $\theta_o$  is not very important as long as it is small (around 0.001 in.). The effect of varying the size of the  $\Delta x$  increment lengths was investigated by the expedient procedure of decreasing the unit Reynolds number from  $10^5$  to  $5 \times 10^4$  per in. This, in essence, halved the  $\Delta x$  increment lengths at a unit Reynolds number of  $10^5$ . The resulting values of  $R_o$  as a function of  $R_x$  (summarized in Table A-2) indicate an effect of only 1% at  $R_x = 10^6$  due to smaller incremental lengths along the flat plate in the integration of Eq. (A-1).

The same integration process used in Eq. (A-1) was performed using the skin-friction formula of Eq. (2) (see Fig. A-1) which is independent of Reynolds number. (Although the ratio of  $C_f/C_{f_i}$  can be assumed independent of Reynolds number,  $C_{f_i}$  is strongly dependent upon Reynolds number.) The results of this integration are summarized in Table A-3 and in Fig. A-2.

As the adiabatic flat-plate, turbulent-boundary-layer relationship of Fig. A-2 ( $R_o$  vs.  $R_x$ ) is quite useful, an attempt was made to obtain an analytical formulation of  $R_o$  as a function of  $R_x$  in order that interpolation of the data could be simplified while retaining a fair degree of accuracy. Based upon the skin-friction law of Eq. (2), the analytical expression relating  $R_o$  to  $R_x$  (based upon the integration procedure discussed previously in this Appendix) is:

$$R_o = A \times B \times C \quad (\text{A-2})$$

where

A is the  $M = 0$  term

B is the  $M$  effect term at  $R_x = 10^6$

C is the  $R_x$  effect on the  $R_o$  term for  $M > 0$  and  $R_x \neq 10^6$

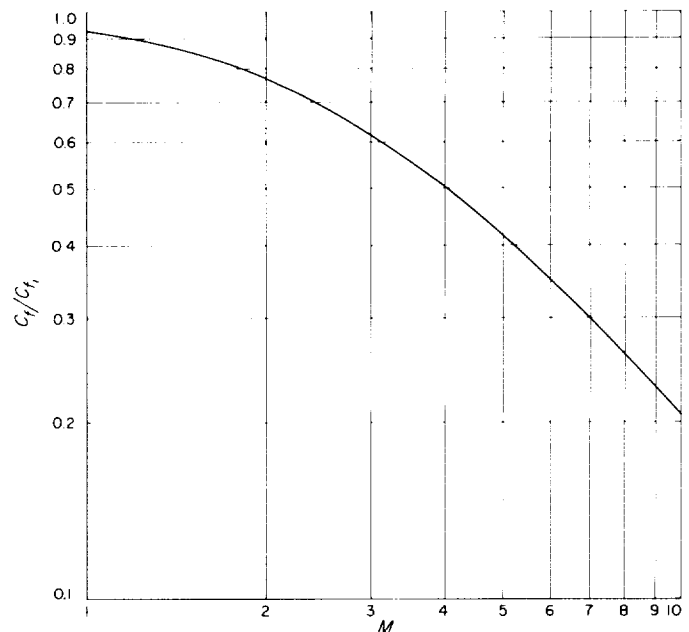


Fig. A-1.  $C_f/C_{f_i}$  vs.  $M$

The actual algebraic forms for A, B, and C are:

$$A = \frac{0.226 R_x}{[1 + 0.033 (\log_{10} R_x - 6.7)] [\log_{10} R_x]^{2.58}} \quad (\text{A-3})$$

$$B = (1 + 0.144 M^2)^{-0.441} \quad (\text{A-4})$$

$$C = \left[ 1 + \frac{M}{300} (\log_{10} R_x - 6) (1 + 0.144 M^2)^{0.441} \right]^{-1} \quad (\text{A-5})$$

The degree to which Eq. (A-2) fits the data of Table A-3 and Fig. A-2 is indicated in Table A-4 where the deviation of the Eq. (A-2) values from the integrated values of  $R_\theta$  vs.  $R_x$  is indicated in per cent for  $0 < M < 6$  and  $5 \times 10^5 < R_x < 10^9$ . For  $R_x \geq 10^6$  the errors are generally less than 2%, a more than satisfactory match of the data by an equation.

The "A" term of Eq. (A-2) is merely an alteration of the Schlichting  $M = 0$  relation [Ref. 12; see Eq. (A-6)] in order to obtain a better fit of the integrated values of the Schultz-Grunow relation of Eq. (1).

$$C_{fi} = \frac{0.455}{(\log_{10} R_x)^{2.58}} \quad (\text{A-6})$$

For  $M = 0$  only, the constant term of Eq. (A-3) should be increased by about 1% yielding one-half the value of

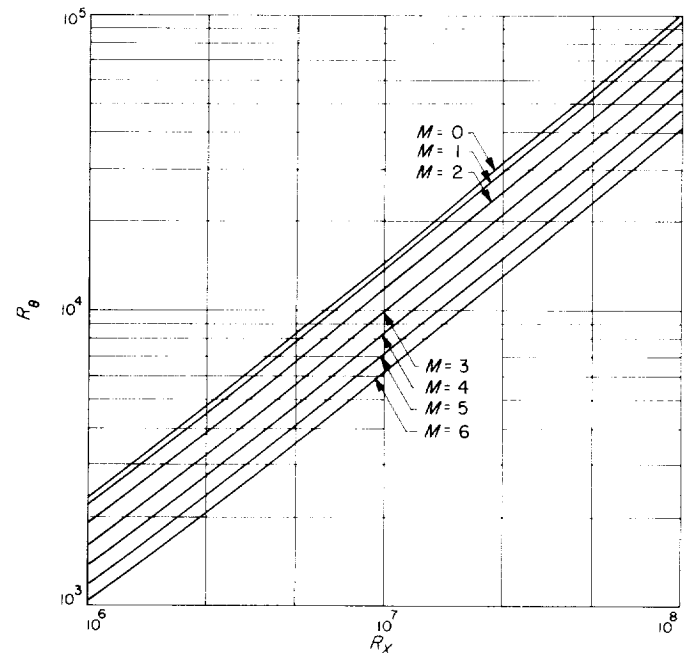


Fig. A-2.  $R_\theta$  vs.  $R_x$  as a function of Mach number [see Eq. (A-2)]

the constant of Eq. (A-6). The "B" term of Eq. (A-2) is simply a minor modification of Eq. (2).

Table A-1. Adiabatic flat-plate, turbulent-boundary-layer properties  
using Eq. (3);  $R/\text{in.} = 10^5$ ,  $\theta_0 = 0.001$  in.

$R_x$	$M = 0$				$M = 1$				$M = 2$				$M = 3$			
	$R_\theta$	$C_f$	$C_f/C_{f_i}$	$R_\theta$	$C_f$	$C_f/C_{f_i}$	$R_\theta$	$C_f$	$C_f/C_{f_i}$	$R_\theta$	$C_f$	$C_f/C_{f_i}$	$R_\theta$	$C_f$	$C_f/C_{f_i}$	$C_f/C_{f_i}$
$2 \times 10^5$	$7.03 \times 10^2$	$4.93 \times 10^{-3}$	1.000	$6.98 \times 10^2$	$4.77 \times 10^{-3}$	0.966	$6.17 \times 10^2$	$4.15 \times 10^{-3}$	0.811	$5.35 \times 10^2$	$3.51 \times 10^{-3}$	0.658	$5.35 \times 10^2$	$3.51 \times 10^{-3}$	0.658	
$5 \times 10^5$	$1.37 \times 10^3$	$4.10 \times 10^{-3}$	1.000	$1.33 \times 10^3$	$3.89 \times 10^{-3}$	0.941	$1.17 \times 10^3$	$3.37 \times 10^{-3}$	0.788	$1.00 \times 10^3$	$2.84 \times 10^{-3}$	0.639	$1.00 \times 10^3$	$2.84 \times 10^{-3}$	0.639	
$1 \times 10^6$	$2.32 \times 10^3$	$3.62 \times 10^{-3}$	1.000	$2.23 \times 10^3$	$3.37 \times 10^{-3}$	0.922	$1.94 \times 10^3$	$2.91 \times 10^{-3}$	0.771	$1.66 \times 10^3$	$2.46 \times 10^{-3}$	0.625	$1.66 \times 10^3$	$2.46 \times 10^{-3}$	0.625	
$2 \times 10^6$	$4.01 \times 10^3$	$3.20 \times 10^{-3}$	1.000	$3.78 \times 10^3$	$2.92 \times 10^{-3}$	0.902	$3.28 \times 10^3$	$2.52 \times 10^{-3}$	0.754	$2.78 \times 10^3$	$2.12 \times 10^{-3}$	0.610	$2.78 \times 10^3$	$2.12 \times 10^{-3}$	0.610	
$5 \times 10^6$	$8.36 \times 10^3$	$2.72 \times 10^{-3}$	1.000	$7.71 \times 10^3$	$2.42 \times 10^{-3}$	0.878	$6.66 \times 10^3$	$2.08 \times 10^{-3}$	0.730	$5.61 \times 10^3$	$1.74 \times 10^{-3}$	0.591	$5.61 \times 10^3$	$1.74 \times 10^{-3}$	0.591	
$1 \times 10^7$	$1.48 \times 10^4$	$2.44 \times 10^{-3}$	1.000	$1.34 \times 10^4$	$2.14 \times 10^{-3}$	0.858	$1.15 \times 10^4$	$1.83 \times 10^{-3}$	0.714	$9.67 \times 10^3$	$1.53 \times 10^{-3}$	0.577	$9.67 \times 10^3$	$1.53 \times 10^{-3}$	0.577	
$2 \times 10^7$	$2.62 \times 10^4$	$2.19 \times 10^{-3}$	1.000	$2.33 \times 10^4$	$1.88 \times 10^{-3}$	0.840	$2.00 \times 10^4$	$1.61 \times 10^{-3}$	0.698	$1.67 \times 10^4$	$1.34 \times 10^{-3}$	0.563	$1.67 \times 10^4$	$1.34 \times 10^{-3}$	0.563	
$5 \times 10^7$	$5.65 \times 10^4$	$1.91 \times 10^{-3}$	1.000	$4.89 \times 10^4$	$1.59 \times 10^{-3}$	0.813	$4.18 \times 10^4$	$1.35 \times 10^{-3}$	0.674	$3.49 \times 10^4$	$1.13 \times 10^{-3}$	0.544	$3.49 \times 10^4$	$1.13 \times 10^{-3}$	0.544	
$1 \times 10^8$	$1.02 \times 10^5$	$1.74 \times 10^{-3}$	1.000	$8.63 \times 10^4$	$1.43 \times 10^{-3}$	0.796	$7.35 \times 10^4$	$1.21 \times 10^{-3}$	0.656	$6.13 \times 10^4$	$1.00 \times 10^{-3}$	0.530	$6.13 \times 10^4$	$1.00 \times 10^{-3}$	0.530	
$2 \times 10^8$	$1.84 \times 10^5$	$1.59 \times 10^{-3}$	1.000	$1.53 \times 10^5$	$1.27 \times 10^{-3}$	0.780	$1.30 \times 10^5$	$1.08 \times 10^{-3}$	0.644	$1.08 \times 10^5$	$8.90 \times 10^{-4}$	0.517	$1.08 \times 10^5$	$8.90 \times 10^{-4}$	0.517	
$5 \times 10^8$	$4.06 \times 10^5$	$1.41 \times 10^{-3}$	1.000	$3.28 \times 10^5$	$1.10 \times 10^{-3}$	0.756	$2.77 \times 10^5$	$9.23 \times 10^{-4}$	0.619	$2.30 \times 10^5$	$7.61 \times 10^{-4}$	0.498	$2.30 \times 10^5$	$7.61 \times 10^{-4}$	0.498	
$1 \times 10^9$	$7.42 \times 10^5$	$1.30 \times 10^{-3}$	1.000	$5.87 \times 10^5$	$9.90 \times 10^{-4}$	0.739	$4.95 \times 10^5$	$8.32 \times 10^{-4}$	0.607	$4.09 \times 10^5$	$6.85 \times 10^{-4}$	0.486	$4.09 \times 10^5$	$6.85 \times 10^{-4}$	0.486	

$R_x$	$M = 4$				$M = 5$				$M = 6$			
	$R_\theta$	$C_f$	$C_f/C_{f_i}$	$R_\theta$	$C_f$	$C_f/C_{f_i}$	$R_\theta$	$C_f$	$C_f/C_{f_i}$	$R_\theta$	$C_f$	$C_f/C_{f_i}$
$2 \times 10^5$	$4.67 \times 10^2$	$2.99 \times 10^{-3}$	0.538	$4.14 \times 10^2$	$2.58 \times 10^{-3}$	0.448	$3.73 \times 10^2$	$2.26 \times 10^{-3}$	0.380	$3.73 \times 10^2$	$2.26 \times 10^{-3}$	0.380
$5 \times 10^5$	$8.63 \times 10^2$	$2.42 \times 10^{-3}$	0.522	$7.56 \times 10^2$	$2.09 \times 10^{-3}$	0.435	$6.73 \times 10^2$	$1.83 \times 10^{-3}$	0.369	$6.73 \times 10^2$	$1.83 \times 10^{-3}$	0.369
$1 \times 10^6$	$1.42 \times 10^3$	$2.09 \times 10^{-3}$	0.510	$1.24 \times 10^3$	$1.80 \times 10^{-3}$	0.425	$1.09 \times 10^3$	$1.58 \times 10^{-3}$	0.360	$1.09 \times 10^3$	$1.58 \times 10^{-3}$	0.360
$2 \times 10^6$	$2.38 \times 10^3$	$1.79 \times 10^{-3}$	0.498	$2.06 \times 10^3$	$1.54 \times 10^{-3}$	0.414	$1.81 \times 10^3$	$1.35 \times 10^{-3}$	0.352	$1.81 \times 10^3$	$1.35 \times 10^{-3}$	0.352
$5 \times 10^6$	$4.77 \times 10^3$	$1.47 \times 10^{-3}$	0.481	$4.12 \times 10^3$	$1.26 \times 10^{-3}$	0.400	$3.61 \times 10^3$	$1.10 \times 10^{-3}$	0.339	$3.61 \times 10^3$	$1.10 \times 10^{-3}$	0.339
$1 \times 10^7$	$8.19 \times 10^3$	$1.29 \times 10^{-3}$	0.470	$7.05 \times 10^3$	$1.10 \times 10^{-3}$	0.390	$6.16 \times 10^3$	$9.61 \times 10^{-4}$	0.330	$6.16 \times 10^3$	$9.61 \times 10^{-4}$	0.330
$2 \times 10^7$	$1.41 \times 10^4$	$1.13 \times 10^{-3}$	0.458	$1.21 \times 10^4$	$9.63 \times 10^{-4}$	0.380	$1.06 \times 10^4$	$8.37 \times 10^{-4}$	0.322	$1.06 \times 10^4$	$8.37 \times 10^{-4}$	0.322
$5 \times 10^7$	$2.94 \times 10^4$	$9.44 \times 10^{-4}$	0.441	$2.51 \times 10^4$	$8.05 \times 10^{-4}$	0.366	$2.19 \times 10^4$	$6.99 \times 10^{-4}$	0.309	$2.19 \times 10^4$	$6.99 \times 10^{-4}$	0.309
$1 \times 10^8$	$5.14 \times 10^4$	$8.38 \times 10^{-4}$	0.430	$4.39 \times 10^4$	$7.14 \times 10^{-4}$	0.357	$3.82 \times 10^4$	$6.18 \times 10^{-4}$	0.302	$3.82 \times 10^4$	$6.18 \times 10^{-4}$	0.302
$2 \times 10^8$	$9.05 \times 10^4$	$7.43 \times 10^{-4}$	0.420	$7.72 \times 10^4$	$6.32 \times 10^{-4}$	0.347	$6.70 \times 10^4$	$5.46 \times 10^{-4}$	0.294	$6.70 \times 10^4$	$5.46 \times 10^{-4}$	0.294
$5 \times 10^8$	$1.92 \times 10^5$	$6.34 \times 10^{-4}$	0.404	$1.63 \times 10^5$	$5.38 \times 10^{-4}$	0.334	$1.41 \times 10^5$	$4.64 \times 10^{-4}$	0.282	$1.41 \times 10^5$	$4.64 \times 10^{-4}$	0.282
$1 \times 10^9$	$3.41 \times 10^5$	$5.70 \times 10^{-4}$	0.393	$2.90 \times 10^5$	$4.82 \times 10^{-4}$	0.326	$2.51 \times 10^5$	$4.16 \times 10^{-4}$	0.274	$2.51 \times 10^5$	$4.16 \times 10^{-4}$	0.274

Table A-2. Effects of  $\theta_0$  and  $R/\text{in.}$  on calculations of  $R_0$  using Eq. (3);  $M=3$ 

$R_x$	$R/\text{in.} = 10^5; \theta_0 = 0.001 \text{ in.}$				$R/\text{in.} = 10^5; \theta_0 = 0.003 \text{ in.}$				$R/\text{in.} = 5 \times 10^4; \theta_0 = 0.001 \text{ in.}$			
	$R_0$	$C_f$	$C_f/C_{f_i}$		$R_0$	$C_f$	$C_f/C_{f_i}$		$R_0$	$C_f$	$C_f/C_{f_i}$	
$2 \times 10^5$	$5.35 \times 10^2$	$3.51 \times 10^{-3}$	0.658		$6.64 \times 10^2$	$3.25 \times 10^{-3}$	0.651		$5.10 \times 10^2$	$3.55 \times 10^{-3}$	0.659	
$5 \times 10^5$	$1.00 \times 10^3$	$2.84 \times 10^{-3}$	0.639		$1.11 \times 10^3$	$2.75 \times 10^{-3}$	0.636		$9.82 \times 10^2$	$2.88 \times 10^{-3}$	0.640	
$1 \times 10^6$	$1.66 \times 10^3$	$2.46 \times 10^{-3}$	0.625		$1.75 \times 10^3$	$2.42 \times 10^{-3}$	0.623		$1.64 \times 10^3$	$2.46 \times 10^{-3}$	0.626	
$2 \times 10^6$	$2.78 \times 10^3$	$2.12 \times 10^{-3}$	0.610		$2.86 \times 10^3$	$2.10 \times 10^{-3}$	0.609		$2.77 \times 10^3$	$2.11 \times 10^{-3}$	0.610	
$5 \times 10^6$	$5.61 \times 10^3$	$1.74 \times 10^{-3}$	0.591		$5.68 \times 10^3$	$1.74 \times 10^{-3}$	0.589		$5.61 \times 10^3$	$1.75 \times 10^{-3}$	0.591	
$1 \times 10^7$	$9.67 \times 10^3$	$1.53 \times 10^{-3}$	0.577		$9.72 \times 10^3$	$1.53 \times 10^{-3}$	0.576		$9.66 \times 10^3$	$1.53 \times 10^{-3}$	0.577	
$2 \times 10^7$	$1.67 \times 10^4$	$1.34 \times 10^{-3}$	0.563		$1.68 \times 10^4$	$1.34 \times 10^{-3}$	0.562		$1.67 \times 10^4$	$1.33 \times 10^{-3}$	0.563	
$5 \times 10^7$	$3.49 \times 10^4$	$1.13 \times 10^{-3}$	0.544		$3.49 \times 10^4$	$1.13 \times 10^{-3}$	0.544		$3.49 \times 10^4$	$1.13 \times 10^{-3}$	0.544	
$1 \times 10^8$	$6.13 \times 10^4$	$1.00 \times 10^{-3}$	0.530		$6.13 \times 10^4$	$1.00 \times 10^{-3}$	0.530		$6.13 \times 10^4$	$1.00 \times 10^{-3}$	0.530	
$2 \times 10^8$	$1.08 \times 10^5$	$8.90 \times 10^{-4}$	0.517		$1.08 \times 10^5$	$8.90 \times 10^{-4}$	0.517		$1.08 \times 10^5$	$8.86 \times 10^{-4}$	0.515	
$5 \times 10^8$	$2.30 \times 10^5$	$7.61 \times 10^{-4}$	0.498		$2.30 \times 10^5$	$7.61 \times 10^{-4}$	0.498		$2.30 \times 10^5$	$7.65 \times 10^{-4}$	0.500	
$1 \times 10^9$	$4.09 \times 10^5$	$6.85 \times 10^{-4}$	0.486		$4.09 \times 10^5$	$6.85 \times 10^{-4}$	0.486					



**Table A-3. Adiabatic flat-plate turbulent-boundary-layer properties  
using Eq. (2);  $R/\text{in.} = 10^5$ ,  $\theta_0 = 0.001$  in.**

$R_x$	$M = 0$		$M = 1$		$M = 2$		$M = 3$	
	$R_\theta$	$C_f$	$R_\theta$	$C_f$	$R_\theta$	$C_f$	$R_\theta$	$C_f$
$2 \times 10^5$	$7.03 \times 10^2$	$4.93 \times 10^{-3}$	$6.65 \times 10^2$	$4.63 \times 10^{-3}$	$5.85 \times 10^2$	$4.00 \times 10^{-3}$	$5.04 \times 10^2$	$3.36 \times 10^{-3}$
$5 \times 10^5$	$1.37 \times 10^3$	$4.10 \times 10^{-3}$	$1.29 \times 10^3$	$3.85 \times 10^{-3}$	$1.12 \times 10^3$	$3.32 \times 10^{-3}$	$9.55 \times 10^2$	$2.79 \times 10^{-3}$
$1 \times 10^6$	$2.32 \times 10^3$	$3.62 \times 10^{-3}$	$2.19 \times 10^3$	$3.40 \times 10^{-3}$	$1.90 \times 10^3$	$2.92 \times 10^{-3}$	$1.60 \times 10^3$	$2.45 \times 10^{-3}$
$2 \times 10^6$	$4.01 \times 10^3$	$3.20 \times 10^{-3}$	$3.77 \times 10^3$	$3.00 \times 10^{-3}$	$3.25 \times 10^3$	$2.57 \times 10^{-3}$	$2.74 \times 10^3$	$2.15 \times 10^{-3}$
$5 \times 10^6$	$8.36 \times 10^3$	$2.72 \times 10^{-3}$	$7.85 \times 10^3$	$2.55 \times 10^{-3}$	$6.76 \times 10^3$	$2.18 \times 10^{-3}$	$5.67 \times 10^3$	$1.82 \times 10^{-3}$
$1 \times 10^7$	$1.48 \times 10^4$	$2.44 \times 10^{-3}$	$1.38 \times 10^4$	$2.29 \times 10^{-3}$	$1.19 \times 10^4$	$1.96 \times 10^{-3}$	$9.95 \times 10^3$	$1.63 \times 10^{-3}$
$2 \times 10^7$	$2.62 \times 10^4$	$2.19 \times 10^{-3}$	$2.46 \times 10^4$	$2.05 \times 10^{-3}$	$2.11 \times 10^4$	$1.75 \times 10^{-3}$	$1.76 \times 10^4$	$1.46 \times 10^{-3}$
$5 \times 10^7$	$5.65 \times 10^4$	$1.91 \times 10^{-3}$	$5.29 \times 10^4$	$1.79 \times 10^{-3}$	$4.53 \times 10^4$	$1.52 \times 10^{-3}$	$3.77 \times 10^4$	$1.27 \times 10^{-3}$
$1 \times 10^8$	$1.02 \times 10^5$	$1.74 \times 10^{-3}$	$9.53 \times 10^4$	$1.63 \times 10^{-3}$	$8.14 \times 10^4$	$1.39 \times 10^{-3}$	$6.77 \times 10^4$	$1.15 \times 10^{-3}$
$2 \times 10^8$	$1.84 \times 10^5$	$1.59 \times 10^{-3}$	$1.72 \times 10^5$	$1.48 \times 10^{-3}$	$1.47 \times 10^5$	$1.26 \times 10^{-3}$	$1.22 \times 10^5$	$1.05 \times 10^{-3}$
$5 \times 10^8$	$4.06 \times 10^5$	$1.41 \times 10^{-3}$	$3.80 \times 10^5$	$1.31 \times 10^{-3}$	$3.23 \times 10^5$	$1.12 \times 10^{-3}$	$2.68 \times 10^5$	$9.25 \times 10^{-4}$
$1 \times 10^9$	$7.42 \times 10^5$	$1.30 \times 10^{-3}$	$6.94 \times 10^5$	$1.21 \times 10^{-3}$	$5.90 \times 10^5$	$1.03 \times 10^{-3}$	$4.89 \times 10^5$	$8.51 \times 10^{-4}$

$R_x$	$M = 4$		$M = 5$		$M = 6$	
	$R_\theta$	$C_f$	$R_\theta$	$C_f$	$R_\theta$	$C_f$
$2 \times 10^5$	$4.39 \times 10^2$	$2.83 \times 10^{-3}$	$3.88 \times 10^2$	$2.43 \times 10^{-3}$	$3.49 \times 10^2$	$2.12 \times 10^{-3}$
$5 \times 10^5$	$8.20 \times 10^2$	$2.35 \times 10^{-3}$	$7.15 \times 10^2$	$2.02 \times 10^{-3}$	$6.34 \times 10^2$	$1.76 \times 10^{-3}$
$1 \times 10^6$	$1.37 \times 10^3$	$2.07 \times 10^{-3}$	$1.18 \times 10^3$	$1.77 \times 10^{-3}$	$1.04 \times 10^3$	$1.54 \times 10^{-3}$
$2 \times 10^6$	$2.33 \times 10^3$	$1.81 \times 10^{-3}$	$2.01 \times 10^3$	$1.55 \times 10^{-3}$	$1.76 \times 10^3$	$1.35 \times 10^{-3}$
$5 \times 10^6$	$4.79 \times 10^3$	$1.53 \times 10^{-3}$	$4.11 \times 10^3$	$1.31 \times 10^{-3}$	$3.59 \times 10^3$	$1.14 \times 10^{-3}$
$1 \times 10^7$	$8.38 \times 10^3$	$1.37 \times 10^{-3}$	$7.18 \times 10^3$	$1.17 \times 10^{-3}$	$6.25 \times 10^3$	$1.01 \times 10^{-3}$
$2 \times 10^7$	$1.48 \times 10^4$	$1.22 \times 10^{-3}$	$1.26 \times 10^4$	$1.04 \times 10^{-3}$	$1.10 \times 10^4$	$9.02 \times 10^{-4}$
$5 \times 10^7$	$3.16 \times 10^4$	$1.06 \times 10^{-3}$	$2.70 \times 10^4$	$8.99 \times 10^{-4}$	$2.34 \times 10^4$	$7.78 \times 10^{-4}$
$1 \times 10^8$	$5.67 \times 10^4$	$9.61 \times 10^{-4}$	$4.82 \times 10^4$	$8.15 \times 10^{-4}$	$4.18 \times 10^4$	$7.05 \times 10^{-4}$
$2 \times 10^8$	$1.02 \times 10^5$	$8.72 \times 10^{-4}$	$8.68 \times 10^4$	$7.40 \times 10^{-4}$	$7.50 \times 10^4$	$6.38 \times 10^{-4}$
$5 \times 10^8$	$2.24 \times 10^5$	$7.70 \times 10^{-4}$	$1.90 \times 10^5$	$6.52 \times 10^{-4}$	$1.64 \times 10^5$	$5.62 \times 10^{-4}$
$1 \times 10^9$	$4.07 \times 10^5$	$7.08 \times 10^{-4}$	$3.45 \times 10^5$	$5.99 \times 10^{-4}$	$2.98 \times 10^5$	$5.16 \times 10^{-4}$

**Table A-4. Percent error<sup>a</sup> of  $R_0$  vs.  $R_x$  of Eq. (A-2) in matching the data of Table A-3**

$R_x$	$M = 0$	$M = 1$	$M = 2$	$M = 3$	$M = 4$	$M = 5$	$M = 6$
$5 \times 10^5$	-4.5	-4.0	-4.5	-4.4	-5.2	-6.2	-6.2
$1 \times 10^6$	-1.7	-1.7	-1.8	-1.6	-1.6	-1.7	-1.8
$2 \times 10^6$	-0.9	-0.5	-0.4	-0.2	-0.1	0	-0.2
$5 \times 10^6$	0.2	0.1	0.8	1.3	1.4	1.5	1.1
$1 \times 10^7$	-0.7	-0.2	0.8	0.7	1.2	1.2	1.4
$2 \times 10^7$	0.7	0.3	1.1	1.9	1.8	2.3	1.8
$5 \times 10^7$	1.0	0.2	0.4	1.3	1.6	1.1	0.4
$1 \times 10^8$	-0.5	-0.1	0.5	0.9	1.3	1.2	-0.2
$2 \times 10^8$	-0.9	-0.9	-0.9	-0.1	0.1	-0.3	-1.2
$5 \times 10^8$	-1.7	-1.6	-0.9	-0.6	-0.9	-1.3	-2.6
$1 \times 10^9$	-1.3	-1.6	-1.1	-0.7	-0.9	-1.4	-3.0

<sup>a</sup>These percent error values are approximate, having been calculated to slide rule accuracy only.

## APPENDIX B

### Short-Cut Method of Estimating Test-Section Boundary-Layer Momentum and Displacement Thickness

The comparisons of the calculations of the test-section boundary layer along the curved wall of the JPL 20-in. SWT with the turbulent boundary-layer growth along an adiabatic flat plate can be used to estimate the corresponding boundary layers of other two-dimensional wind tunnels. Table B-1 compares the adiabatic flat-plate, turbulent boundary layer (based upon the distance from the throat to the boundary-layer station in the test section, and assuming test-section Mach number and Reynolds number throughout) to the measured values in the test section. These ratios are plotted in Fig. B-1 along with similar results from several other facilities, both smaller and larger.

The ratios of Fig. B-1 in conjunction with the  $H/H_0$  values of Fig. 6 can be combined to give rough estimations of the curved-wall, turbulent-boundary-layer momentum and displacement thickness in the test section. The flat-plate boundary-layer data of Table A-3, Fig. A-2 or Eq. (A-2) are used for the ratios of Fig. B-1. The results of these calculations are shown in Tables B-2, B-3, and B-4 for the JPL 12-in. SWT (Ref. 8), CIT Co-op Wind Tunnel (Ref. 13), and the AEDC 40-in. SWT (Refs. 14, 15). These boundary-layer momentum-thickness estimations are generally good to within about 5%. However, the displacement thicknesses based upon this simple method are off by as much as 13%, and, in gen-

eral, are never better than about 5%. The reasons for these discrepancies can be seen from Figs. B-1 and B-2.

The relationship between  $\theta_{fp}$  and  $\theta$  measurements in Fig. B-1 is not monotonic with tunnel size, as the JPL 20-in. SWT curve is straddled by the curves obtained from larger facilities. Comparing the data as a function

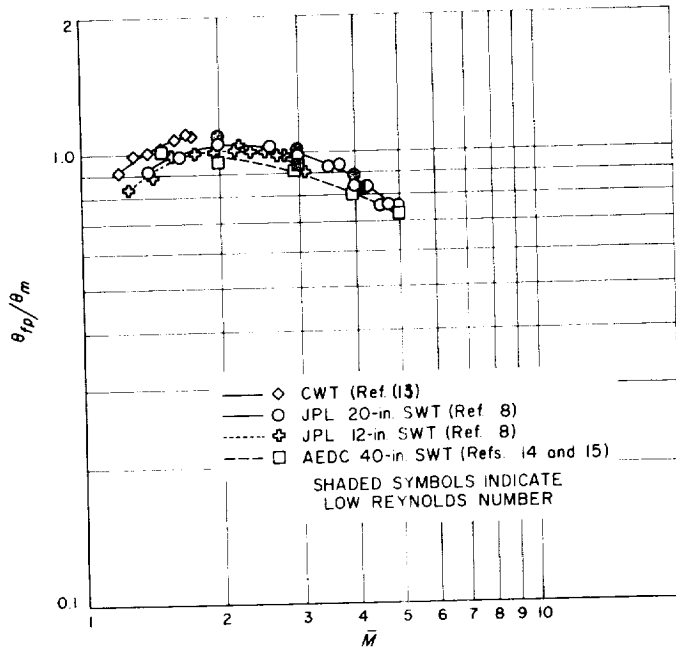


Fig. B-1.  $\theta_{fp}/\theta_m$  vs.  $\bar{M}$  for several supersonic wind tunnels

of tunnel test-section  $R_x$  does not offer any more hope than the use of tunnel size. Perhaps a universal (average) curve would be the most suitable. It is quite definite that in a given facility, the curve moves upward with decreasing Reynolds number.

The ratios of  $H/H_0$  in Fig. B-2 appear to be monotonic with tunnel size, and in a given facility, the curve is raised with a decrease in Reynolds number. Perhaps a better estimate of  $\delta^*$  can be made by allowing for the effect of tunnel size than was obtained by simply using the results from the JPL 20-in. SWT shown in Fig. 6.

The basic relationships of the short-cut method are as follows:  $R_\theta$  is a function of  $R_x$  and  $M$  [Eq. (A-2) or Fig. A-2]. Use  $\bar{M}$  for  $M$ .  $R_x$  is based on: (a) distance from nozzle throat to test-section boundary-layer station; (b) test-section Mach number ( $\bar{M}$ ); and (c) test-section unit Reynolds number ( $R/in.$ ).

$$\theta_{fp} = \frac{R_\theta}{R/in.}$$

$$\theta_{calc} = \theta_{fp} / \frac{\theta_{fp}}{\theta_m}$$

$$\delta^*_{calc} = \theta_{calc} \times H_0 \times \frac{H_m}{H_0}$$

The value of  $\theta_{fp}/\theta_m$  is from the JPL 20-in. SWT curve in Fig. B-1. The value of  $H_m/H_0$  is from the JPL 20-in. SWT curve in Fig. B-2.

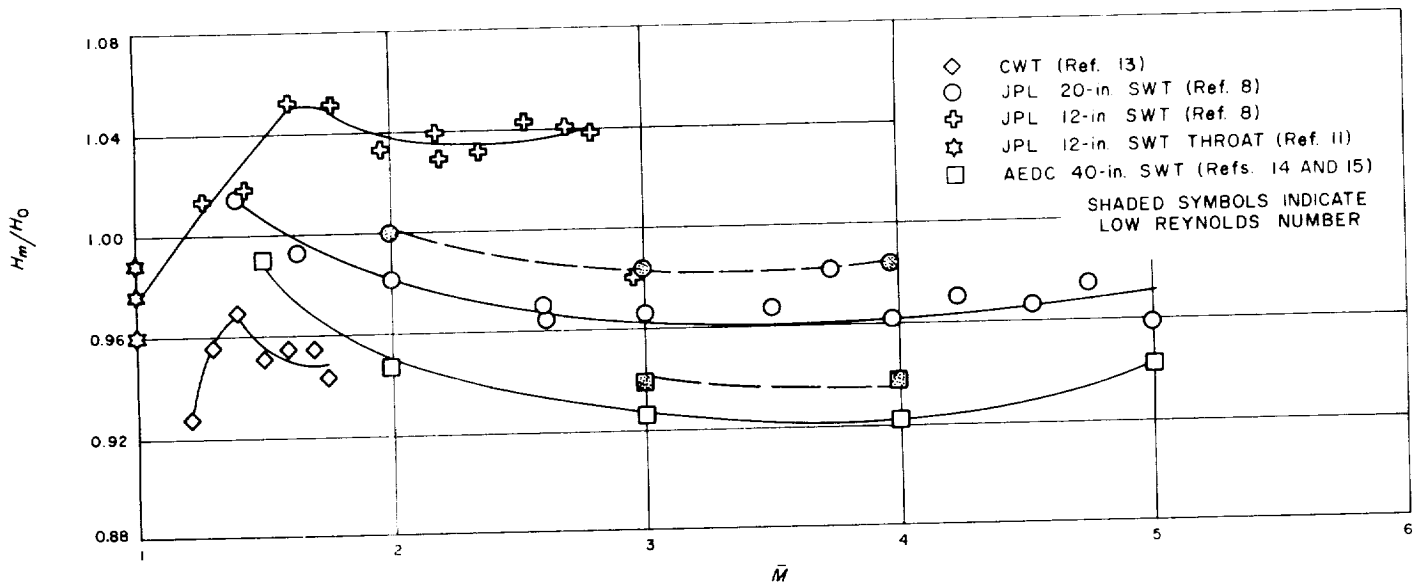


Fig. B-2. Normalized values of the measured boundary-layer parameter,  $H$ , from several supersonic wind tunnels

Table B-1. JPL 20-in. SWT test-section boundary-layer measurements  
on centerline of curved wall

$M$	$R/\text{in.}$ $\times 10^{-5}$	$x$ in.	$R_x$ $\times 10^{-7}$	$\delta_m^*$ in.	$\theta_m$ in.	$H_m$	$R_\theta \times 10^{-4}$ (flat plate)	$\theta_{fp}$ in.	$\frac{\theta_{fp}}{\theta_m}$
1.40	5.10	66.1	3.37	0.171	0.0769	2.23	3.59	0.0705	0.917
1.64	4.99	78.9	3.94	0.201	0.0797	2.52	3.94	0.0785	0.985
2.01	1.39	92.4	1.28	0.302	0.0958	3.15	1.46	0.1050	1.097
2.01	5.01	92.4	4.63	0.249	0.0804	3.10	4.24	0.0848	1.055
2.61	3.65	105.2	3.84	0.371	0.0868	4.27	3.23	0.0885	1.021
2.61	3.70	103.8	3.84	0.364	0.0845	4.31	3.23	0.0873	1.033
3.00	1.38	112.0	1.54	0.548	0.1030	5.32	1.42	0.1029	0.998
3.00	3.32	112.0	3.72	0.476	0.0903	5.27	2.95	0.0889	0.985
3.50	3.34	117.1	3.91	0.603	0.0899	6.71	2.80	0.0838	0.933
3.74	3.18	118.3	3.76	0.660	0.0866	7.63	2.59	0.0815	0.942
3.98	1.23	118.9	1.46	0.883	0.1050	8.42	1.14	0.0927	0.882
3.98	3.29	118.9	2.90	0.765	0.0924	8.28	2.58	0.0784	0.848
4.23	3.54	118.9	4.21	0.823	0.0891	9.23	2.65	0.0749	0.841
4.54	3.36	118.9	4.00	0.983	0.0944	10.41	2.41	0.0717	0.760
4.76	3.02	118.6	3.58	1.052	0.0921	11.42	2.12	0.0703	0.764
5.00	2.45	118.4	2.90	1.136	0.0926	12.27	1.72	0.0703	0.760
							Comparison with flat-plate boundary layer.		

Table B-2. JPL 12-in. SWT test-section boundary-layer measurements  
on centerline of curved wall

$M$	$R/\text{in.}$ $\times 10^{-5}$	$x$ in.	$R_x$ $\times 10^{-7}$	$\delta_m^*$ in.	$\theta_m$ in.	$H_m$	$R_\theta \times 10^{-4}$ (flat plate)	$\theta_{fp}$ in.	$\theta_{calc}$ in.	$\delta_{calc}^*$ in.	$\frac{\theta_{calc}}{\theta_m}$	$\frac{\delta_{calc}^*}{\delta_m^*}$
1.27	5.62	36.5	2.05	0.107	0.0517	2.07	2.42	0.0431	0.0487	0.099	0.94	0.93
1.43	5.77	42.5	2.45	0.123	0.0539	2.28	2.76	0.0478	0.0510	0.115	0.95	0.94
1.61	5.92	47.5	2.81	0.134	0.0512	2.62	2.98	0.0504	0.0515	0.127	1.01	0.95
1.78	5.93	50.5	2.99	0.150	0.0518	2.90	3.06	0.0516	0.0504	0.138	0.97	0.92
1.97	5.51	53.0	2.92	0.165	0.0520	3.18	2.90	0.0527	0.0507	0.152	0.98	0.92
2.18	5.29	55.0	2.91	0.186	0.0515	3.62	2.77	0.0524	0.0504	0.172	0.98	0.92
2.20	6.20	45.9	2.85	0.153	0.0423	3.62	2.73	0.0440	0.0423	0.145	1.00	0.95
2.36	6.38	47.0	3.00	0.170	0.0427	3.98	2.77	0.0434	0.0417	0.157	0.98	0.92
2.54	6.54	47.9	3.13	0.184	0.0415	4.44	2.75	0.0421	0.0408	0.169	0.98	0.92
2.70	6.78	48.7	3.30	0.205	0.0424	4.84	2.82	0.0416	0.0407	0.182	0.96	0.89
2.80	6.75	49.1	3.31	0.213	0.0419	5.09	2.77	0.0411	0.0403	0.191	0.96	0.90
2.98	6.87	49.7	3.41	0.229	0.0435	5.27	2.77	0.0403	0.0409	0.213	0.94	0.93
							Estimation of test-section boundary layer using results of JPL 20 in.-SWT measurements.					

**Table B-3. CWT test-section boundary-layer measurements on  
centerline of curved wall**

$M$	$R/\text{in.}$ $\times 10^{-5}$	$x$ in.	$R_x$ $\times 10^{-7}$	$\delta_m^*$ in.	$\theta_m$ in.	$H_m$	$R_\theta \times 10^{-4}$ (flat plate)	$\theta_{fp}$ in.	$\theta_{calc}$ in.	$\delta_{calc}^*$ in.	$\frac{\theta_{calc}}{\theta_m}$	$\frac{\delta_{calc}^*}{\delta_m^*}$
1.21	1.61	240	3.86	0.519	0.284	1.83	4.14	0.258	0.293	0.588	1.03	1.13
1.30	1.40	240	3.37	0.515	0.261	1.98	3.63	0.259	0.270	0.558	1.03	1.08
1.40	1.49	240	3.58	0.531	0.252	2.11	3.77	0.253	0.263	0.597	1.04	1.12
1.50	1.48	240	3.55	0.541	0.243	2.22	3.68	0.248	0.248	0.595	1.02	1.10
1.60	1.32	240	3.18	0.548	0.232	2.36	3.30	0.250	0.245	0.617	1.06	1.13
1.70	1.33	240	3.20	0.558	0.222	2.51	3.27	0.246	0.239	0.633	1.08	1.13
1.75	1.29	240	3.10	0.572	0.224	2.55	3.16	0.245	0.236	0.647	1.05	1.13
							Estimation of test-section boundary layer using results of JPL 20-in. SWT measurements.					

**Table B-4. AEDC 40-in. SWT test-section boundary-layer measurements  
on centerline of curved wall**

$M$	$R/\text{in.}$ $\times 10^{-5}$	$x$ in.	$R_x$ $\times 10^{-7}$	$\delta_m^*$ in.	$\theta_m$ in.	$H_m$	$R_\theta \times 10^{-4}$ (flat plate)	$\theta_{fp}$ in.	$\theta_{calc}$ in.	$\delta_{calc}^*$ in.	$\frac{\theta_{calc}}{\theta_m}$	$\frac{\delta_{calc}^*}{\delta_m^*}$
1.5	1.96	214.5	4.21	0.415	0.180	2.31	4.25	0.181	0.189	0.442	1.05	1.06
2	3.50	214	7.48	0.475	0.160	2.97	6.37	0.152	0.148	0.467	0.93	0.98
3	1.75	215	3.76	0.92	0.180	5.11	29.7	0.170	0.170	0.915	0.94	1.00
3	5.25	215	11.30	0.78	0.155	5.03	7.51	0.143	0.144	0.761	0.93	0.98
4	0.93	215	2.01	1.54	0.190	8.11	1.49	0.159	0.177	1.52	0.93	0.99
4	5.00	215	10.70	1.18	0.148	7.97	6.00	0.120	0.139	1.17	0.94	0.99
5	5.67	214	12.10	1.65	0.137	12.04	5.67	0.100	0.135	1.66	0.99	1.00
These measurements estimated from plotted results in Refs. 14 and 15.							Estimation of test-section boundary layer using results of JPL 20-in. SWT calculations.					

## REFERENCES

1. Coles, Donald, *Measurements in the Boundary Layer on a Smooth Flat Plate in Supersonic Flow*, Section III. "Measurements in a Flat-Plate Boundary Layer at the Jet Propulsion Laboratory," Report No. 20-71, Jet Propulsion Laboratory, Pasadena, June 1, 1953.
2. Korkegi, R. H., *Transition Studies and Skin Friction Measurements on an Insulated Flat Plate at a Hypersonic Mach Number*, Memorandum HWT 17, Guggenheim Aeronautical Laboratory, California Institute of Technology, Pasadena, July 15, 1954.
3. Lobb, Kenneth R., Eva M. Winkler, and Jerome Persh, "Experimental Investigation of Turbulent Boundary Layers in Hypersonic Flow," *Journal of the Aeronautical Sciences*, Volume 22, No. 1, January, 1955.
4. Brinich, P. F., and N. S. Diaconis, *Boundary Layer Development and Skin Friction at Mach Number 3.05*, National Advisory Committee for Aeronautics TN 2742, July, 1952.
5. O'Donnell, R. M., *Experimental Investigation at a Mach Number of 2.41 of Average Skin-Friction Coefficients and Velocity Profiles for Laminar and Turbulent Boundary Layers and an Assessment of Probe Effects*, National Advisory Committee for Aeronautics TN 3122, January, 1954.
6. Hakkinen, Raimo J. (Aakko), *Measurements of Turbulent Skin Friction on a Flat Plate at Transonic Speeds*, National Advisory Committee for Aeronautics TN 3486, September, 1955.
7. Winkler, Eva M. and Moon H. Cha, "Experimental Investigations of the Effect of Heat Transfer on Hypersonic Turbulent Boundary-Layer Skin Friction," *Journal of the Aeronautical Sciences*, Vol. 26, No. 2, February, 1959.
8. Dayman, Bain, Jr., "Summary of Boundary Layer Measurements Made on the Test Section Walls of the JPL Supersonic Wind Tunnels," Internal Memorandum WT G-C1, Jet Propulsion Laboratory, Pasadena, December, 1960.
9. Schultz-Grunow, F., *New Frictional Resistance Law for Smooth Plates*, National Advisory Committee for Aeronautics Technical Memorandum 986; In this report  $C_{f_i}$  is given as a function of  $R_x$ . Also see Ludwig, H., and W. Tillman, *Investigations of the Wall-Shearing Stress in Turbulent Boundary Layers*, National Advisory Committee for Aeronautics Technical Memorandum 1285, May, 1950; In this report  $C_{f_i}$  is given as a function of  $R_\theta$ .
10. Reshotko, Eli and Maurice Tucker, *Approximate Calculation of the Compressible Turbulent Boundary Layer with Heat Transfer and Arbitrary Pressure Gradient*, National Advisory Committee for Aeronautics TN 4154, December, 1957.
11. Sibulkin, Merwin, *Boundary-Layer Measurements at Supersonic Nozzle Throats*, Report No. 20-97, Jet Propulsion Laboratory, Pasadena, May, 1956.
12. Schlichting, H., *Boundary Layer Theory*, McGraw-Hill, New York, 1955.

## REFERENCES (Cont'd)

13. Pounder, Edwin, "Boundary Layer Measurements in the Cooperative Wind Tunnel," private communique, California Institute of Technology, Pasadena.
14. Jones, Jerry, *An Investigation of the Boundary-Layer Characteristics in the Test Section of a 40 by 40-inch Supersonic Tunnel*, Arnold Engineering Development Center TN-60-189, (VKF, ARO, Inc.), Tullahoma, Tennessee, October, 1960.
15. Schueler, C. J. and W. T. Strike, *Calibration of a 40-inch Continuous Flow Tunnel at Mach Numbers 1.5 to 6*, Arnold Engineering Development Center TN-59-136, (VKF, ARO, Inc.), Tullahoma, Tennessee, November, 1959.

## NOMENCLATURE

$C_f$	compressible local skin-friction coefficient	$x$	distance from: 1) throat of nozzle 2) leading edge of flat plate
$C_{fi}$	incompressible local skin-friction coefficient	$\Delta x$	incremental value of $x$
$H$	$\delta^*/\theta$	$\delta^*$	boundary-layer displacement thickness
$H_0$	nominal $H = 1.3 + 0.46M^2$	$\theta$	boundary-layer momentum thickness
$L^*$	nozzle throat radius of curvature	$\theta_{fp}$	turbulent boundary-layer momentum thickness for adiabatic flat plate
$M$	Mach number: 1) along nozzle 2) over flat plate	$\theta_0$	boundary-layer momentum thickness at nozzle throat
$\bar{M}$	test-section Mach number	$\theta_{ts}$	test-section boundary-layer momentum thickness as calculated by boundary-layer momentum equation
$P_t$	supply-section pressure	$\nu^*$	air viscosity in nozzle-throat boundary layer based on average of wall and freestream temperatures
$R$	Reynolds number	$( )_{calc}$	calculated values using short-cut method of Appendix B
$R/in.$	Reynolds number per inch	$( )_m$	measured values
$R_x$	length Reynolds number $= xR/in.$		
$R_0$	momentum Reynolds number $= \theta R/in.$		
SWT	supersonic wind tunnel		
$t^*$	nozzle throat height		
$T_t$	supply-section temperature		

